Atomic Fluorescence Yields

R. W. FINK
School of Chemistry, Georgia Institute of Technology, Atlanta, Georgia

R. C. JOPSON, HANS MARK, C. D. SWIFT
Lawrence Radiation Laboratory, University of California, Livermore, California

The mechanisms of the reorganization of atoms with inner shell vacancies are reviewed. All available experimental values of K-, L-, and M-shell fluorescence yields, together with L-shell Coster–Kronig yields are summarized and compared with available theoretical calculations. Rather good agreement exists in general between theory and experiment for the K shell, but experimental values of the L_2 and L_3 subshell fluorescence yields disagree substantially with the semitheoretical results of Listengarten. Related phenomena in μ-mesic atoms are included. Experimental methods of measurement are summarized and discussed, together with suggestions for future studies with high resolution techniques. Results from the literature have been included up to 10 May 1966.

1. INTRODUCTION AND DEFINITIONS

1.1. Fluorescence and Auger Yields

The creation of a vacancy in an atomic shell initiates a series of rearrangement processes which may become quite complicated. A single vacancy created, for example, in the K shell is filled in a time of the order of 10^{-17}–10^{-14} sec by an electron coming from some higher shell (e.g., the L_2 subshell), thus shifting the vacancy to the higher shell. The difference in binding energy between the two shells (e.g., the $K-L_2$ energy difference) either is released as a K x-ray photon or is transferred to another bound electron (e.g., an L_3 electron) which is ejected (e.g., a $K-L_2L_3$ Auger transition). This results in an atom with two vacancies. Continuation of these processes gives rise to the emission of L, M, N, etc. x rays and Auger electrons, resulting in an atom with multiple vacancies in its outermost shells; i.e., a highly charged ion. In principle, both the radiative and the Auger process are well understood. The radiative transitions can be adequately explained in terms of multipole theory which predicts that by far the most important mode is the electric dipole, although other multipoles also may cause observable effects. The nonradiative, or Auger, transitions occur because of the Coulomb interaction existing among the different electrons in the atom (Be-64). Detailed theories exist which can accurately predict nonradiative transition rates (As-59, As-65, Li-60, Li-62, Di-63, Ca-63b, a).

High resolution spectrometry has made it possible to determine the binding energies of a vast number of atomic levels (2-Ha-64), but the transition rates between levels and the branching ratios between different decay modes are not nearly as well known. The present review summarizes the situation existing today in a restricted class of these branching ratios—the atomic fluorescence yields and Coster–Kronig yields.

Historically, the fluorescence yield of an element was defined in terms of the intensity of fluorescent radiation produced when a sample of the material was exposed to a beam of energetic x rays. More recently, it has been defined in terms of the probability that a vacancy in a given shell results in a radiative transition. The fluorescence yield of the ith subshell of an atom, ω_i, is the probability that a vacancy in that subshell is filled by a radiative transition. The Auger yield of the same shell, a_i, is defined as the probability that an electron is emitted when the vacancy is filled from a higher shell. Great care must be taken in applying these definitions in practical situations because several complicated rearrangements may occur before the vacancy is filled. These definitions can be applied in a straightforward manner to the K shell, which consists of two $s_{\frac{1}{2}}$ electrons. The fluorescence yield of the K shell, ω_K, can thus be obtained by measuring the number of characteristic K x rays emitted per K-shell vacancy. Since the K shell has only one subshell, the

experiment results in a quantity directly related to the fluorescence yield as defined above.

1.2. Subshell Yields and Coster–Kronig Transitions

The situation is more complicated in the case of higher atomic shells. In the L shell, for instance, there are eight electrons grouped into three subshells (L_1, L_2, and L_3) each of which corresponds to a different quantum state. The fluorescence yield of each of these subshells can be defined as before; however, two circumstances make it difficult to apply the definition in practical situations:

(1) In most experiments it is very difficult to ionize only one of the three L subshells. Usually, all three subshells are ionized in some specific ratio, so that the L shell fluorescence yield measured in a typical experiment is an average fluorescence yield ($\bar{\omega}_L$). Since the fluorescence yields of the three subshells (ω_1, ω_2, and ω_3) generally are not equal, the mean fluorescence yield, $\bar{\omega}_L$, will depend on the ratio of the number of primary vacancies produced in the three subshells and thus on the way in which the L shell is ionized.

(2) A second complicating factor is that in certain regions of the periodic table, radiationless transitions occur that move a vacancy in one L subshell to another ($L_1 \rightarrow L_3$, $L_1 \rightarrow L_2$, or $L_2 \rightarrow L_3$). Therefore, a primary vacancy which originally is created in the L_1 shell may move to the L_2 or L_3 shell before it is filled by an electron from a higher (M, N, etc.) shell. These transitions are called Coster–Kronig transitions (Co-35), and they complicate the situation by changing the distribution of primary vacancies among the three subshells. Great care must be taken to insure that this effect is properly included in the calculation of the subshell yields ω_1, ω_2, and ω_3 from measured average fluorescence yield, $\bar{\omega}_L$.

In the case of fluorescence yields for shells higher than the L shell, the situation is even more complex. The M shell, for example, has five subshells which may be ionized each with different probabilities by the primary excitation process. After the initial ionization, Coster–Kronig transitions may redistribute the primary vacancies before these are filled by electrons from higher shells. If all of the M subshells are ionized, there may be eight or ten different processes before the event is over. To trace all of these in detail is quite complicated (Di-63). Since very little experimental data on M- or higher-shell fluorescence yields are available, not much attention can be given to these complications other than to mention that they exist.

1.3. Quantitative Relationships and Notation

To make certain that various experiments are properly interpreted, it is important that a uniform notation system be employed. There is a fairly large literature on L-shell fluorescence yields for which the notation system is rather well standardized. The relationships between the various important quantities will be developed here for the L shell to account for the two complications discussed in the preceding section. These are the existence of subshells (in shells above the K shell) and the possibility that radiationless transitions between the subshells change the initial distribution of primary vacancies.

In an L-shell fluorescence yield experiment in which vacancies are created in all three subshells and no Coster–Kronig transitions occur, an average L-fluorescence yield is measured. This average fluorescence yield may be expressed in terms of the individual subshell fluorescence yields as

$$\bar{\omega}_L = N_1\omega_1 + N_2\omega_2 + N_3\omega_3, \tag{1}$$

where N_1, N_2, and N_3 are the relative numbers of primary vacancies in the three subshells, respectively. It follows that

$$N_1 + N_2 + N_3 = 1 \tag{2}$$

and it is easy to see that Eq. (1) is consistent with the general definition of the fluorescence yield given in Sec. 1.1. Since the quantities of theoretical interest are the subshell fluorescence yields ω_1, ω_2, and ω_3, it is clear that no information about these can be obtained from Eq. (1) unless further measurements are made. In general, it is necessary to perform two other measurements of mean L-fluorescence yields, $\bar{\omega}_L'$ and $\bar{\omega}_L''$ for *different* ratios of primary vacancies $N_1' : N_2' : N_3'$ and $N_1'' : N_2'' : N_3''$. If all of the primary vacancy distributions are known, then the subshell fluorescence yields ω_1, ω_2, and ω_3 can be calculated from the set of equations

$$\begin{aligned} \bar{\omega}_L &= N_1\omega_1 + N_2\omega_2 + N_3\omega_3 \\ \bar{\omega}_L' &= N_1'\omega_1 + N_2'\omega_2 + N_3'\omega_3 \\ \bar{\omega}_L'' &= N_1''\omega_1 + N_2''\omega_2 + N_3''\omega_3. \end{aligned} \tag{3}$$

It is clear that in any L-shell fluorescence yield experiment, the determination of the subshell vacancy distribution is as important as the measurement of the mean L-fluorescence yield itself.

Equations (1), (2), and (3) are applicable only if the primary vacancy distribution remains unaltered before the vacancies are filled by transitions from higher shells. If Coster–Kronig transitions (Co-35) occur within the subshell, then the situation is more complicated. Under such circumstances, two views are possible: One is to regard the measured mean L-fluorescence yield, $\bar{\omega}_L$, as a linear combination of the subshell fluorescence yields ω_1, ω_2, and ω_3, with a vacancy distribution altered by Coster–Kronig transitions. This is the view taken by Listengarten (Li-60). The other view is to let the mean L-fluorescence yield, $\bar{\omega}_L$, be a linear combination of the *primary* vacancy distribution N_1, N_2, and N_3 and to redefine the fluorescence yields of the subshells to account for the Coster–Kronig transitions, as was done by Wapstra, Nijgh, and van Lieshout (Wa-59). The latter system is some-

what more convenient from the experimental viewpoint, since the equations are written in terms of the primary vacancy distribution $N_1:N_2:N_3$, which is usually known in a given experiment. It is important to recognize that the two notation systems are completely equivalent. The appropriate transformation equations between them will now be developed.

If the mean L-fluorescence yield is regarded as a linear combination of the three subshell yields, ω_1, ω_2, and ω_3, then it may be expressed as:

$$\bar{\omega}_L = V_1\omega_1 + V_2\omega_2 + V_3\omega_3. \tag{4}$$

The coefficients V_1, V_2, and V_3 represent a modified vacancy distribution in which Coster–Kronig processes are taken into account. It should be noted that

$$V_1 + V_2 + V_3 \geq 1. \tag{5}$$

The N's are relative primary vacancy distributions and thus, by definition, obey Eq. (2). Because of the way the fluorescence yields are defined, the condition (5) applies to the V's, because some of the vacancies created in the L_1 and L_2 subshells must be counted twice since they may be shifted to higher shells. The final vacancy distribution $V_1:V_2:V_3$ can be rewritten in terms of the primary vacancy distribution $N_1:N_2:N_3$ using the appropriate Coster–Kronig yields,

$$\begin{aligned} V_1 &= N_1 \\ V_2 &= N_2 + f_{12}N_1 \\ V_3 &= N_3 + f_{23}N_2 + (f_{13} + f_{12}f_{23})N_1, \end{aligned} \tag{6}$$

where f_{12}, f_{13}, and f_{23} are the respective probabilities for the occurrence of the Coster–Kronig transitions $L_1 \rightarrow L_2$, $L_1 \rightarrow L_3$, and $L_2 \rightarrow L_3$. Listengarten (Li-60) also defines three other quantities which are often useful,

$$\begin{aligned} X_1 &= V_1\omega_1, \\ X_2 &= V_2\omega_2, \\ X_3 &= V_3\omega_3. \end{aligned} \tag{7}$$

The quantities X_1, X_2, and X_3 are the respective fractions of x-ray quanta emitted per *total* L-shell vacancy with energies corresponding to transitions *to* each of the L subshells.

If the mean L-fluorescence yield is expressed in terms of the primary vacancy distribution, the following equation results:

$$\bar{\omega}_L = N_1\nu_1 + N_2\nu_2 + N_3\nu_3. \tag{8}$$

The coefficients ν_1, ν_2, and ν_3, denoted as ν_{L_I}, $\nu_{L_{II}}$, and $\nu_{L_{III}}$ by Wapstra, Nijgh, and van Lieshout (Wa-59), are specially defined "fluorescence yields." The quantity ν_1 is the fraction of *all* L x rays observed per vacancy in the L_1 subshell. Note that this is quite different from the definition of the actual fluorescence yield for that subshell ω_1, when it is required that the L x-ray transitions go *only* to the L_1 subshell. It is instructive at this point to emphasize that the products $V_i\omega_i$, called X_i by Listengarten (Li-60), and $N_i\nu_i$ are *not* equal. Only the sums of the products for all three subshells are equal to the mean fluorescence yield $\bar{\omega}_L$, [see Eqs. (4) and (8)]. This is obvious from the respective physical definitions: The product $V_i\omega_i$ (or X_i) represents the number of L x rays filling vacancies in the ith subshell per vacancy in the entire L shell. The product $N_i\nu_i$, on the other hand, represents the number of L x rays observed per vacancy created in the ith subshell. It is readily seen from Eqs. (8), (6), and (4) that the relations between the quantities ν_1, ν_2, and ν_3 and ω_1, ω_2, and ω_3 are

$$\begin{aligned} \nu_1 &= \omega_1 + f_{12}\omega_2 + (f_{13} + f_{12}f_{23})\omega_3, \\ \nu_2 &= \omega_2 + f_{23}\omega_3, \\ \nu_3 &= \omega_3. \end{aligned} \tag{9}$$

In some of the early papers in this field (Kü-35), before the mechanism of Coster–Kronig transitions was discovered (Co-35), no distinction was made between the ν's and the ω's. This has led to some confusion, since some of the values quoted as "subshell fluorescence yields" in certain tables (Bu-52) are in fact ν's and not ω's.

It is obvious from the foregoing discussion that a determination of the three subshell yields ω_1, ω_2, and ω_3 may be a fairly complex procedure. If Coster–Kronig yields are included, a set of simultaneous equations such as the set (3) is obtained, except that instead of the primary vacancy distributions N_1, N_2, N_3, the more complicated expressions given in Eq. (6) must be employed. In general, three different mean L-fluorescence yields measured for three different primary vacancy distributions *and* the appropriate Coster–Kronig yields must be known to deduce values of ω_1, ω_2, and ω_3. Fortunately, the conditions can often be adjusted to reduce the complexity. It is generally possible to measure ω_3 alone using the critical excitation method (Sec. 2.5). Furthermore, there are certain regions of the periodic table for which some of the Coster–Kronig yields are small so that the equations can be greatly simplified (see Sec. 3.2).

As yet, no mention has been made of the Auger yields, which are the complementary quantities to the fluorescence yields. The fluorescence yield ω_i has been defined as the probability that a vacancy in the ith subshell is filled by an electron making a radiative transition. The Auger yield a_i is the probability that a vacancy in the ith shell is filled with an electron making a nonradiative transition *from a higher shell* (see Sec. 3.1). The underlined phrase in the definition is important, since the Coster–Kronig transitions are *excluded* from the definition of the Auger yields. The Coster–Kronig yield is the probability that a vacancy is filled with an electron making a nonradiative transition from a *higher subshell* in the *same* major shell (see Sec. 3.2). From these definitions, it is obvious that

the following relations must hold between the fluorescence yields, the Auger yields, and the Coster–Kronig yields for the L shell:

$$\omega_3+a_3=1,$$
$$\omega_2+a_2+f_{23}=1,$$
$$\omega_1+a_1+f_{12}+f_{13}=1. \quad (10)$$

The expressions for mean L-shell Auger yields can be developed in precisely the same way as for the fluorescence yields. In the Listengarten notation (Li-60),

$$\bar{a}_L=a_1V_1+a_2V_2+a_3V_3=A_1+A_2+A_3. \quad (11)$$

It can be shown from Eqs. (10), (6), and (4) that the sum of the mean fluorescence yield and the mean Auger yield for the *same* initial vacancy distribution is

$$\bar{a}_L+\bar{\omega}_L=1. \quad (12)$$

Another important fact should be mentioned at this point. The total "width" of an energy level (i.e., an inner shell vacancy in an atom) is the sum of the partial widths of all of the processes by which the level can decay (i.e., processes by which the vacancy can be filled). Thus,

$$\Gamma_{T_i}=\Gamma_{X_i}+\Gamma_{a_i}+\sum_{k>i}\Gamma_{ik}, \quad (13)$$

where Γ_{T_i} is the total width, Γ_{X_i} the radiation width, and Γ_{a_i} is the Auger width for the ith subshell. The quantities Γ_{ik} are the widths for the Coster–Kronig transitions $k\rightarrow i$. From the definitions of ω_i, a_i, and f_{ik}, it can be seen that (Ki-48a)

$$\omega_i=\Gamma_{X_i}/\Gamma_{T_i},$$
$$a_i=\Gamma_{a_i}/\Gamma_{T_i},$$
$$f_{ik}=\Gamma_{ik}/\Gamma_{T_i}. \quad (14)$$

The method of using radiation width measurements has been employed to determine fluorescence and Auger yields at high Z (see Sec. 5.1).

In addition to the system developed above for the fundamental quantities dealt with in this review, there are several other derived quantities which are important enough to deserve special attention. A partial L-shell fluorescence yield which is often used is the fluorescence yield of the L shell following K x-ray emission, ω_{KL}. The quantity ω_{KL} may be defined as

$$\omega_{KL}=N_2\nu_2+N_3\nu_3, \quad (15)$$

where $N_2=(K_{\alpha_2}/K_\alpha)$ and $N_3=(K_{\alpha_1}/K_\alpha)$, the ratio of K_{α_2} and K_{α_1} x rays to the total K_α x-ray emission, respectively.

Another quantity often determined experimentally is the partial L-shell fluorescence yield following L-electron capture, ω_{LL}. The quantity ω_{LL} depends on ω_1, ω_2, ω_3, and the Coster–Kronig yields f_{12}, f_{13}, and f_{23}. Since for allowed and first-forbidden L capture, $N_1\approx 1$ and N_2, $N_3\ll 1$ (RF-55, RF-60), we define ω_{LL} as

$$\omega_{LL}\approx\nu_1=\omega_1+f_{12}\omega_2+(f_{13}+f_{12}f_{23})\omega_3. \quad (16)$$

In general, one may think of ω_{KL} as a special case of the mean L-fluorescence yield $\bar{\omega}_L$ for which $N_1\approx 0$, and of ω_{LL} as a special case of $\bar{\omega}_L$ for which $N_1\approx 1$. The quantity ω_{LL} is particularly important in most electron capture and in certain internal conversion experiments because these processes create vacancies predominantly in the L_1 subshell.

2. CREATION OF PRIMARY VACANCIES

2.1. Photoelectric Absorption

The primary vacancies in most fluorescence yield measurements are usually produced by bombarding the atom with photons, electrons, or with heavy charged particles of sufficient energy to cause ionization. The vacancies also can be produced by such radioactive decay processes as electron capture and internal conversion. If the shell to be ionized consists of more than one subshell, then each of these processes results in a different distribution of primary vacancies. Furthermore, the distribution may also depend on the energy of the incident radiation or particles.

Most of the early work on fluorescence yields was performed using photoelectric ionization to create the primary vacancies. (Indeed, the name "fluorescence yield" came from the fact that the measurement involves the observation of fluorescent x rays during the irradiation of a sample.) The measurements of K-shell fluorescence yields were performed using the schematic geometry shown in Fig. 1. The detector A observes the fluorescent x rays, and the detector B measures the transmitted beam. When the sample is removed, detector B measures the incident beam intensity. The difference in the observed intensities is a measure of the attenuation in the target and thus depends on the rate

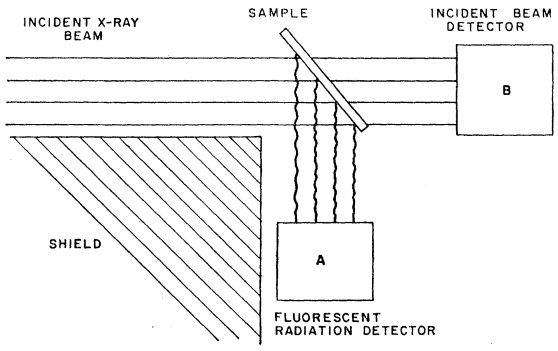

FIG. 1. A schematic arrangement for measuring fluorescence yields. The x-ray detector B may be used either to measure the attenuation of the incident beam by the sample or the intensity of the incident beam with the sample removed. The x-ray detector A is used to measure the intensity of the fluorescent radiation from the sample.

at which vacancies are created by the incident beam. When this is compared with the counting rate observed in detector A, the fluorescence yield can be calculated according to the definition given in Sec. 1.1. In practice, it is not enough simply to measure the attenuation, since too many other mechanisms can lead to absorption of x rays from the incident beam. Even the very early workers in the field (La-34) used theoretical estimates to calculate the fraction of the incident x rays which cause vacancies in the appropriate atomic shells. Fortunately, theoretical values of the ionization cross sections (or partial absorption coefficients) for the K shell are well known over a wide energy region, so that the necessary calculations can easily be performed if the spectrum of the incident radiation is known. For a complete discussion, see C. M. Davisson (Da-64). The reliance upon theoretical values for the computation of the creation of primary vacancies is justified for the K shell.

In the case of higher atomic shells, however, it is necessary to know not only the total absorption coefficient, but also how the vacancies created are distributed among the subshells. In the case of the L shell, for instance, this is necessary if some information about the actual subshell yields ω_1, ω_2, and ω_3 is desired. The best discussion of vacancy creation by photoionization of the L shell is given by Ross, Cochran, Hughes, and Feather (Ro-55). If relatively soft x rays are used to ionize the L shell (i.e., x rays with quantum energies between two and five times the mean binding energy of the L-shell electrons), the ratio of primary vacancies is approximately $N_1:N_2:N_3=1:2:3$. This ratio was obtained from several experimental measurements quoted in Ro-55, and it should not be considered as being very reliable. Indeed, the photoelectric method of creating vacancies in higher shells has not been extensively employed precisely because the subshell vacancy ratio is difficult to determine. Recently, a number of more effective methods (see Secs. 2.2, 2.3, and 2.4) of creating vacancies in higher shells have been developed, where it is possible to determine the vacancy ratio with greater accuracy. Consequently, photoelectric excitation of L- and higher-shell vacancies is no longer used extensively for precise measurements of subshell fluorescence yields.

2.2. Ionization by Impact of Electrons and Heavy Charged Particles

Electron beams have been employed to produce primary vacancies for fluorescence yield measurements. This method has the drawback that it is generally not possible to measure the rate of vacancy creation directly, but that it must be calculated using the theory of ionizing collisions. Fortunately, such calculations can be performed quite accurately for a variety of incident electron energies (Be-30, Be-33).

The electron beam current must be determined accurately if the appropriate fluorescence yield is to be calculated. This is accomplished by placing the target in a biased Faraday cup to eliminate the effect of secondary electrons on the current observed. In such experiments, the fluorescence yield is determined by comparing the observed x-ray intensity with the yield calculated on the assumption that all vacancies are filled by radiative transitions.

For measurements in higher atomic shells, the primary vacancy distribution among the subshells also must be determined. For electron energies far above the ionization potential, the ratio of vacancies is proportional simply to the electron population in each subshell. Thus, for the L subshells, the vacancy ratio is approximately $N_1:N_2:N_3=1:1:2$. For lower energies, a more precise calculation of the vacancy ratio is necessary. Bethe (Be-30, Be-33) has developed a theoretical expression from which the relative ionization in the various L subshells due to electron bombardment can be calculated. For electrons having kinetic energies greater than 40 keV,

$$N_1:N_2:N_3=(1/E_1):(1/E_2):(2/E_3), \qquad (17)$$

where E_1, E_2, and E_3 are the respective binding energies of the L_1, L_2, and L_3 subshells. This formula has been verified experimentally to within 15% in bombardments with electrons having energies greater than 40 keV (Vi-61).

Heavy charged particles can also be employed for primary vacancy creation. Cross sections for x-ray production for many elements using protons and alpha-particles with energies between 0.1 and 4.3 MeV have been measured (Ge-37, Jo-62, Le-53). However, no measurements of fluorescence yields have been attempted. The reason for this situation is that the calculation of the vacancy creation rate using available theoretical models for heavy charged particles is not reliable for incident particle energies below some 10 to 20 times the ionization energy (Jo-62). Thus, while it is relatively easy to observe characteristic x rays emitted by targets bombarded with heavy charged particles, there is no precise way of computing the fluorescence yield from these data. If more accurate theoretical calculations of ionization cross sections were available, then the heavy charged particle excitation could become a very useful method for obtaining fluorescence yields from measurements of x-ray intensities during bombardment. One advantage is that the characteristic x rays produced are free of the usual bremsstrahlung background present when electron bombardment is used. The very high intensity, low-energy ion accelerators now being built (Ma-64) could be employed to great advantage. The x rays produced by such machines are of sufficient intensity that high resolution diffraction spectrometers could be employed to separate x-ray transitions leading to vacancies in different subshells. This point will be amplified in greater detail in Sec. 4.

2.3. Ionization of Higher Shells by Transitions to K-Shell Vacancies

A method which has been developed recently to to determine L- and M-shell fluorescence yields is to use the L- and M-shell vacancies produced by transitions to vacancies in the K shell, which usually are produced by photoelectric absorption (Jo-63, Jo-64, a, b), but also may be created by other means (Ho-63, Ho-64). The radiative transitions to the K-shell vacancies are employed as a signal to indicate the presence of a vacancy in one of the higher shells. This method has several advantages over those employed previously for determining L-shell fluorescence yields. The primary vacancy distribution in the L subshells is determined precisely by the relative intensities of the K_α x rays ($N_1:N_2:N_3 \approx 0:1:2$), so that no theoretical estimates are required to determine the proper primary vacancy distribution. Precise values of the vacancy ratios are given in Wapstra, Nijgh, and van Lieshout (Wa-59). Furthermore, since each L-shell vacancy is preceded by a K_α x ray, coincidence measurements can be used to measure the fluorescence yield of the L shell. The mean L-fluorescence yield ω_{KL} will be determined by the coincidence rate observed between the L and the K x rays. Therefore, no theoretical calculation is necessary to determine the number of primary vacancies—the K_α x ray serves as a marker that the vacancy is in place. This method of creating primary vacancies also has been employed to determine certain M-shell mean fluorescence yields (Jo-65). In these experiments, the L shell was ionized by photon bombardment, and the coincidence rate between the L and the M x rays emitted by the foil was determined. The results of these measurements are discussed in Sec. 5.3.

2.4. Ionization by Electron Capture or Internal Conversion

Electron capture and internal conversion also produce primary vacancies in atomic shells. Electron capture processes particularly are useful, because the primary vacancy distribution usually is known from the nature of the transition (RF-55, RF-60). Moreover, each transition usually is accompanied by an x ray or a gamma ray which can be employed to mark the existence of a vacancy in much the same way that the K x rays were employed in the method described in Sec. 2.3. A good example is the isotope W^{181} (Jo-61). This isotope decays by electron capture to the ground state predominantly, but also to excited levels at 152 and 137 keV. The fact that about one-third of W^{181} decays lead to the first excited state of Ta^{181} at 6.3 keV does not alter the conclusion that the L-shell vacancies created in this decay are predominantly in the L_1 subshell. The 6.3-keV transition is not converted in the L shell and the electron capture transition from W^{181} to the 6.3-keV level, as well as to the ground state, is allowed. The ground state transition can proceed by K electron capture, giving a Ta^{181} atom ionized in the K shell. The coincidence rate between K and L x rays can be used to determine the same fluorescence yield (ω_{KL}) of the L shell as before, since it does not matter how the K shell is ionized.

The decay to the excited nuclear levels can be employed (Ra-65b) to measure a slightly different partial fluorescence yield. If the decay energy is not large enough to permit transitions to the excited levels by K-electron capture, then all of these transitions must cause vacancies in the L or higher atomic shells. In the case of allowed and first-forbidden transitions, almost all of the primary vacancies are created in the L_1 subshell. The coincidence rate between the gammas emitted in the nuclear decay process and the L x rays thus determines a different partial L-shell fluorescence yield (ω_{LL}), defined in Sec. 1.3, than that measured using the K capture to the ground state. This illustrates the necessity of knowing the primary vacancy distribution to determine the precise partial fluorescence yield in measurements of shells above the K shell. It also demonstrates how a knowledge of nuclear decay schemes may be used to determine primary vacancy distributions.

Internal conversion processes also ionize various atomic shells. A nuclear state decaying by K conversion may be used to determine ω_{KL} in a manner similar to K capture. The L conversion also may be employed to determine M-shell fluorescence yields by measuring L and M x-ray coincidence rates. The coincidence method between gammas and L x rays cannot be employed since, in general, no unique gamma ray accompanies an L conversion event. As is the case for electron capture processes in higher shells, the primary vacancy distribution in the L shell (and higher shells) produced by internal conversion is determined by the properties of the nuclear decay. An electric quadrupole (E2) transition, for example, will not lead to the same distribution of L-shell vacancies as a transition having a different multipole order. There is also a difference between electric and magnetic multipole orders. Owing to these complications, electron capture transitions are generally more useful than internal conversion for fluorescence yield determinations.

If a particular decay scheme is really well known, or if theory can be applied with great confidence, then it is unnecessary to use the coincidence methods described here. For such cases, the number of primary vacancies can be determined by measuring the decay rate of the source using one of the other radiations emitted (α, β, or γ) and then using the known decay scheme to calculate the number of primary vacancies produced per decay. For example, $[(\alpha)(L \text{ x ray})]$ coincidences were used for plutonium (Sa-61), together with $L_2:L_3$ x-ray intensities.

2.5. Critical Excitation of Specific Subshell Vacancies

It has been shown that for higher atomic shells the vacancy distribution usually depends on the method of

excitation. In some of the very early experiments, attempts to control the vacancy distribution more precisely were made (Kü-35, St-37). For example, it is relatively easy to determine ω_3, the fluorescence yield of the L_3 subshell. This subshell is the least tightly bound L subshell. By adjusting the energy of the incident radiation or particles appropriately, it is possible to excite vacancies only in the L_3 subshell and thus to determine ω_3. In the experiments quoted in Kü-35 and St-37, this was done by fixing the energy of the incident bremsstrahlung beam so that the endpoint of the spectrum fell between the L_2- and L_3-subshell binding energies. In principle, the method of critical excitation described here can be extended to measure ω_2 and ω_1. If the endpoint energy of the incident bremsstrahlung spectrum is made to lie between the L_2 and the L_1 subshells, then vacancies in the L_2 and L_3 subshells only will be produced. The mean L-fluorescence yield measured in this way will be a linear combination of ω_2 and ω_3. Since ω_3 will be known from the previous measurement, ω_2 can be computed if the vacancy distribution and the Coster–Kronig yield f_{23} are known. In principle, the method can be extended to determine ω_1 if the vacancy distribution and the appropriate Coster–Kronig yields are known (Ro-54). In practice, the critical excitation method is useful primarily for the determination of ω_3, since uncertainties in the primary vacancy distribution make measurements of ω_2 and ω_1 unreliable.

An interesting variation of the critical excitation method has been employed with the K and L x-ray coincidence technique described in Sec. 2.3. The L shell vacancy distribution following K_α x-ray emission is $N_1:N_2:N_3=0:1:2$. The average fluorescence yield, ω_{KL}, determined by this method is the appropriate linear combination of the L_2 and L_3 subshell fluorescence yields defined in Eq. (15) with $N_2:N_3=1:2$,

$$\omega_{KL}\approx 1/3\omega_2+2/3\omega_3. \tag{18}$$

This average yield is measured because the K x-ray detector cannot resolve the K_{α_1} and the K_{α_2} x rays. (The K_{α_1} line is the transition $L_3\rightarrow K$, and the K_{α_2} line is the transition $L_2\rightarrow K$.) The coincidence method also can be employed to measure ω_3 separately. Instead of observing the K x rays directly, the K x-ray detector now is shielded from the direct radiations from the sample. A radiator foil is placed in the direct sample beam and the K x-ray counter is set to observe the radiator. For certain materials, it is possible to choose the radiator in such a way that the K shell of the radiator atoms can be ionized only by the K_{α_1} and not by the K_{α_2} x rays emitted by the sample. A signal observed in the K x-ray counter therefore indicates a vacancy in the L_3 shell, and hence the coincidence rate observed will be proportional to ω_3. If ω_{KL} is also known, then ω_2 can be calculated using Eq. (18). This method of determining ω_2 and ω_3 has been applied successfully to several elements in the region between $Z=67$ and $Z=83$ (Jo-64a). (The possibility of using high-resolution detection to resolve the K_{α_1} and K_{α_2} x rays will be discussed in Sec. 4.)

3. REARRANGEMENT OF VACANCIES

3.1. Shifting of Vacancies between Major Shells

In the filling of a K-shell vacancy by an electron of a higher shell, the vacancy of course reappears in the higher shell. The number of L-shell vacancies produced in the filling of a K-shell vacancy is n_{KL} (RF-55, RF-60) and is given by

$$n_{KL}=k\omega_K+a_K\left\{\left[\frac{2(K-LL)+(K-LX)}{\sum \text{Auger electrons}}\right]\right\} \tag{19}$$

where k is K_α/K, the ratio of K_α x-ray intensity to the total K series x-ray intensity, a_K is the K shell Auger yield $(1-\omega_K)$, and $(K-LX)$ is a partial Auger yield where X denotes $M-$, $N-$, etc. shell electrons. For example, $K-LX$ is the probability that a K-shell vacancy is filled by an L-shell electron with the binding energy difference transferred to an electron in the X shell which is ejected. Values of n_{KL} have been computed by Robinson and Fink (RF-55, RF-60) and by Listengarten (Li-60). A similar quantity f_{KL_i} given by Wapstra, Nijgh, and van Lieshout (Wa-59) is related to n_{KL} by the relation

$$n_{KL}=\sum f_{KL_i}. \tag{20}$$

Similarly, the fraction of K vacancies shifted to the M shell is n_{KM}, and the fraction of L-shell vacancies shifted to the M shell is n_{LM}. Owing to the paucity of data on partial L-shell Auger electron yields, accurate values of n_{LM} are not yet available.

The appearance in higher shells of vacancies shifted up in the course of filling lower shells is important in experiments where a fluorescence yield is measured by determining the relative intensities of emitted x rays or Auger electrons, as for example in electron capture excitation (Sec. 2.4). The relative intensities of L and K x rays, I_L/I_K, have been measured for several electron capturers, for which the orbital electron capture ratio, P_L/P_K, is known either from direct measurement or from computation from the electron capture decay energy (Q_{EC}). A mean L-fluorescence yield is then obtained by means of the relation (Fi-55)

$$\bar{\omega}_L=\frac{(I_L/I_K)\omega_K}{(P_L/P_K+n_{KL})}. \tag{21}$$

In principle, mean M-shell fluorescence yields can be obtained in a similar manner from measurements of M, L, and K x-ray intensities, with account being taken of P_M/P_L, the ratio of probabilities for $M-$ and $L-$ capture, P_L/P_K, n_{KL}, n_{KM}, and n_{LM}. No measurements of M-shell fluorescence yields by this method have been reported to date.

3.2. Shifting of Vacancies among Subshells: Coster–Kronig Transitions

Radiationless transitions occurring within a subshell are of great importance in the measurements of fluorescence yields other than ω_K. These transitions alter the initial distribution of primary vacancies, and they must be taken into account in the computation of individual subshell yields from measured average fluorescence yields for the entire shell. The formal way in which this effect is included in the equations has been discussed (for the L shell) in Sec. 1.3, and the Coster–Kronig transition probabilities f_{13}, f_{12}, and f_{23} have been defined (again for the L shell).

There are two important points regarding the magnitude and the behavior of the Coster–Kronig yields which must be understood. One is that the radiationless transition probabilities for the shifting of vacancies between subshells are of the same order of magnitude as the radiative transition probabilities for filling the vacancies from *higher* shells. If this were not the case, then the initial vacancy distribution produced in a given experiment would not be altered *before* the vacancies were filled by radiative processes. There is abundant evidence that rearrangements within the shell do, in fact, occur before the atom radiates (Bu-52).

The second point is that the actual magnitudes of the Coster–Kronig transition rates tend to vary strongly with atomic number. If a vacancy is shifted from a lower subshell to a higher one, then an energy equal to the difference between these levels must be released. This energy is transferred to an electron in a higher shell by the Coulomb interaction.

Thus, Coster–Kronig transitions are Auger transitions in which the vacancy shifts from one subshell to another within a given shell (Co-35). In the general Auger case, the radiative and nonradiative transition rates are comparable, but in the Coster–Kronig case, the radiative transition rates among the subshells are negligible compared to nonradiative ones. Thus, no x rays corresponding to transitions of the type $L_1 \rightarrow L_2$, etc., are observed (Bu-52), but the effects of nonradiative transitions cannot be ignored. Recently, direct observation of low-energy electrons (<1 keV) from L-shell Coster–Kronig transitions has been reported (Al-61, Va-62) as well as from the M shell (Me-65) A Coster–Kronig process is characterized by the two subshells between which the vacancy shift occurs and the electron in the higher shell which removes the energy. The process is usually denoted in the manner, for example, $L_1-L_3M_4$, which means that a vacancy has shifted from the L_1 to the L_3 subshell, and that the binding energy difference released has been removed by an M_4 electron which is ejected from the atom, leaving a vacancy in the M_4 shell. Whether or not such a process can occur with a large probability depends upon whether an electron is energetically available in the next higher shell to absorb the energy. If all of the M electrons, for instance, have binding energies larger than the energy differences between the L subshells, then Coster–Kronig yields are generally very small, since it is more difficult to transfer the transition energy to an electron in the N or even a higher shell. The situation outlined here explains why Coster–Kronig yields tend to vary strongly as a function of atomic number. In certain regions of the periodic table all M electrons have higher binding energies than the energy differences between the L subshells. In these regions, the Coster–Kronig yields will be small (less than 0.1). In other regions, M electrons may be ejected in Coster–Kronig processes, and thus the yields may be quite large (≈ 0.7). This "threshold" effect thus accounts for the observed variation of the Coster–Kronig yields. See Table XIII in Burhop (Bu-52).

Several theoretical calculations and experimental measurements of Coster–Kronig yields have been performed which are of use in computing subshell fluorescence yields from measured average fluorescence yields. The method employed in the calculation is identical to that introduced by Wentzel (We-27) for the calculation of Auger electron emission rates. The most recent calculations are those by Callan (Ca-63a) and Asaad (As-65), who computed the Coster–Kronig yields for the transitions $L_1L_{2,3}-M_{4,5}$. (It should be noted that these are not quite the same as the *total* Coster–Kronig yields f_{12} and f_{13}, because only those transitions in which the electron ejected is in the M_4 or M_5 levels are considered.) The results exhibit the characteristic behavior of Coster–Kronig yields in that the values have a strong dependence on atomic number. It was shown also that the magnitudes of the calculated Coster–Kronig yields depend quite critically on the electronic wave functions used to compute the matrix elements. Unfortunately, the calculations of Callan are available only between $Z=21$ and $Z=50$. Many of the measurements for which a precise knowledge of the Coster–Kronig yields are needed are for values of $Z \geq 50$, so that these calculations cannot be employed.

For heavier atoms, there are a number of experimental values of Coster–Kronig yields which are available. Ferreira, Costa, Concalves, and Salguero (Fe-65) have determined the f_{13} Coster–Kronig yields for six elements between $Z=73$ and $Z=92$ by comparing the intensities of L x-ray lines with L_α and L_{β_2} satellite lines. Dionisio (Di-63) has measured soft Auger electron spectra emitted in the decays of Em^{220} (thoron) and Em^{222} (radon). The Coster–Kronig yields, f_{12} and f_{13}, for Po, Bi, Pb, and Tl have been calculated from these data. Very recently, Melhorn (Me-65) has reported the first measurement of an M-shell Coster–Kronig yield ($M_2-M_{3,4}N_5$) in krypton. This yield was deduced from the measured Auger electron spectrum resulting from irradiating krypton with monoenergetic electrons at two different energies, 2000-eV and 290-eV incident energy. The experimental result agrees

qualitatively with theoretical predictions that the probability for a Coster–Kronig transition is much greater than for an Auger transition, if the former is energetically possible.

A summary of all available Coster–Kronig yields is given in Table IV in Sec. 5.2. More extensive measurements and calculations of Coster–Kronig yields for a broader range of elements are urgently needed.

4. FILLING OF VACANCIES AND MEASUREMENT OF AUGER ELECTRON AND X-RAY INTENSITIES

4.1. Auger Electron Measurements

Precision beta-spectrometers have been used for many years to measure the energies and intensities of Auger electrons. The latest review of this work is that of Bergström (Be-64), as mentioned in Sec. 1.1. Electron intensity measurements have been most useful in determining K-shell fluorescence yields by comparing the intensities of the electron transitions to the total linewidth. Auger electron measurements have not been used extensively for the determination of fluorescence yields of higher atomic shells because the electron energies resulting from the filling of higher shell vacancies generally are too low. Since excellent discussions of electron spectroscopy are available (Si-64), no detailed description of the experiments for the measurement of K-shell fluorescence yields will be given. Some of the features of the ω_K experiments will be discussed in Sec. 5.1 to compare the measurements with theory.

Many of the L-shell measurements using electron spectrometry have been performed by Haynes and his collaborators (Na-60, Bu-58, 2-Ha-55, Le-58). A good example of an L-Auger electron spectrum obtained with a medium resolution lens spectrometer is shown in Fig. 7 of Ref. Na-60. Measurements of $\bar{a}_L$ and $\bar{\omega}_L$ for Hg are described in this paper (Na-60).

A novel variation of the electron technique was used by Päschke (Pä-63) to measure $\bar{a}_L$, ω_1, ω_2, and ω_3 for Au. A 50-Å foil was suspended in a beam of 55-keV electrons. This foil was located between the poles of a magnetic spectrometer. Electrons from the primary beam were collected in a Faraday cup and the Auger electrons were bent through collimating slits between the poles and detected 180° from the foil in a Geiger counter. Simultaneously, the L x rays from the foil were detected by a NaI(Tl) crystal spectrometer looking between the poles. A drawing of the experimental arrangement is shown in Fig. 2. The Auger spectrum and the L x-ray spectrum provide enough information, along with the measured efficiency of the equipment, to determine the Auger and the fluorescence yields.

4.2. X-Ray Intensity Measurements

A great many methods for measuring the x-ray intensities in fluorescence yield experiments have been developed. These fall into two large categories, those involving the use of high-resolution spectrometers, and the large majority of measurements in which low-resolution devices are employed. The advantage of using high-resolution equipment is of course that it is then possible to investigate the shape and intensity of each individual transition in a spectrum of characteristic x rays. Unfortunately, diffraction spectrometers have very low efficiencies and it is necessary, therefore, to use very intense sources, or else data must be taken for long periods of time. In addition, this low efficiency usually rules out the possibility of using the diffraction spectrometer as one of the two detectors in a coincidence-type experiment.

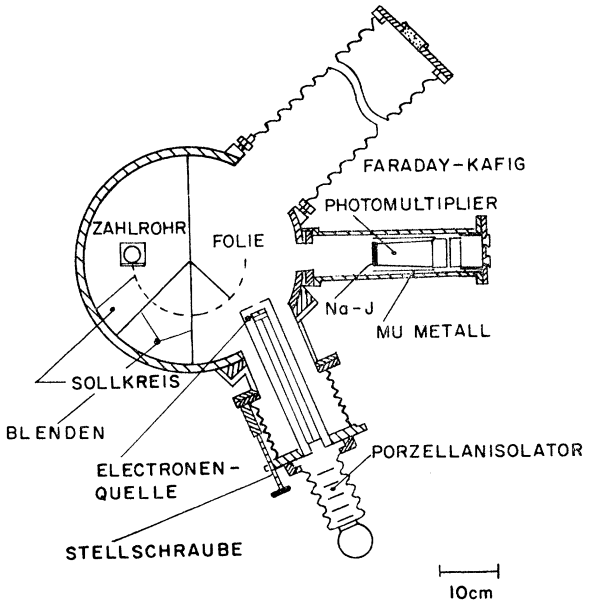

FIG. 2. The experimental arrangement used by Päschke (Pä-63) for the measurement of fluorescence and Auger yields in gold. The magnetic field is perpendicular to the plane of the paper. The Auger electrons emitted by the sample foil mounted in the chamber are counted with the proportional counter inside the vacuum chamber, and the L x rays are detected by the scintillation counter mounted on the right side of the chamber.

Low-resolution devices have in common the advantage of high efficiency and convenience of use. These detectors can in practice be designed to have efficiencies of 100% in a 4π geometry. The low resolution of these detectors makes it impossible to separate and investigate individual transitions, except in a few isolated cases where critical absorption techniques are usable, or where peculiar vacancy populations occur. In the remainder of this section, a number of examples illustrating how the various x-ray detectors are employed will be discussed. In addition, an attempt will be made to evaluate the potentialities of some of the newer developments in the field of radiation detection.

4.2.1. Photographic Detection of X Rays

Although this technique is no longer employed, it is of some historical interest, since some of the first

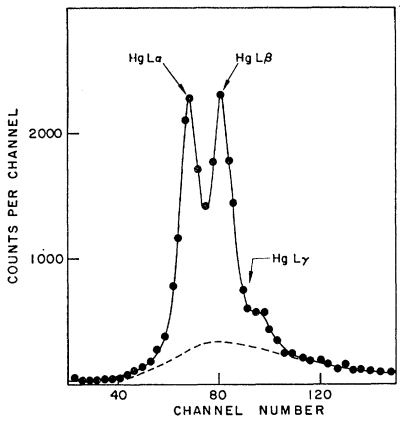

FIG. 3. The L x-ray spectrum of mercury as observed with a proportional counter obtained by Rao and Crasemann (Ra-64) is shown. A 9:1 mixture of argon and methane was used as the counter gas. Pressures ranging from 30 to 160 Torr were used. The x rays entered the counter through a 0.005-in.-thick beryllium window.

comprehensive measurements of both K- and L-shell fluorescence yields were performed using photographic plates to measure x-ray intensities. H. Lay in 1934 (La-34) used photographic plates to determine both the intensity of the incident beam and fluorescent radiation by measuring the time ratio necessary to obtain roughly equal darkening of the film and then making the appropriate corrections for the difference in film efficiency for the incident and fluorescent radiation. In view of the uncertainties involved in the photographic method, it is remarkable how well Lay's results have stood the test of time; 32 years later, Lay's values of ω_K and $\bar{\omega}_L$ are still considered to be among the better measurements of these quantities.

4.2.2. *Ionization Chambers and Geiger Counters*

Another series of early measurements were those made using ionization chambers to detect the primary and the fluorescent radiation. Küstner and Arends (Kü-35) and Stephenson (St-37) used variations of the ionization chamber technique to measure the ratio of fluorescent radiation to the primary beam intensity. In each case, the vacancy production rate was computed from the measured primary beam intensity. Calibrated Geiger–Müller counters with known spectral responses were used by Kinsey (Ki-48b) to detect L x rays from Pb^{212} (ThB) to measure an L-fluorescence yield.

4.2.3. *Proportional Counters*

The development of proportional counters has made it possible to resolve x-ray lines caused by the filling of vacancies in specific shells. At 10 keV, a good proportional counter may have a resolution of 10 to 15% of the incident quantum energy. It is possible therefore to resolve partially the L_α, L_β, and L_γ x-ray groups at high Z (see Fig. 3). The most common use of the proportional counter, however, is to separate the L x rays from the K x rays emitted by a given atom. The L-shell fluorescence yields thus have been measured by using proportional counters to determine the x-ray intensity, and by making a separate measurement or calculation of the number of vacancies (Ro-55, Fi-57). A recent example of this is the experiment of Zimmerli and Flammersfeld (Zi-63) to determine the L-fluorescence yield of Dy. The experiment consisted of measuring the conversion electrons from the decay of Dy^{165m} (1.26 min). These electrons were counted in an anthracene crystal spectrometer. Assuming the conversion coefficients are known, the intensity of the conversion electrons gives the number of vacancies in the L shell. By then counting the L x rays detected in the proportional counter, the L-shell fluorescence yield is determined.

In another example of this method, Winkenbach (Wi-58) measured mean L-fluorescence yields of thallium ($Z=81$) and bismuth ($Z=83$) from the decay of Pb^{212}–Bi^{212}–Tl^{208} series (Th–B–C–C″). Here the ionization in the L shell is known accurately from the conversion in bismuth of the 238-keV gamma in Pb^{212} decay, and in thallium from conversion of the 40-keV gamma following Bi^{212} α-decay. Thus, a proportional counter determination of the total intensity of the L x rays emitted from Pb^{212} (ThB) and Bi^{212} (ThC) sources measures the mean L-fluorescence yields of bismuth and thallium, respectively. Furthermore, by partially resolving the L_α, L_β, and L_γ x rays in Bi^{212} decay, the fluorescence yield for the L_3 shell of thallium was found, $\omega_3=0.33\pm0.02$ (Wi-58).

An interesting variation of the proportional counter method is to employ internally mounted sources of radiation. These can be either radioisotopes or atoms in the counter gas (or wall) used as fluorescent radiators. The internal source method was employed by Konstantinov *et al.* (Ko-60, Ko-61, Ko-64, Ko-65) to measure fluorescence yields in Ga, Cu, V, and Mn for the L shell, and in V, Mn, Cu, Ga, Mg, and Al for the K shell. Similar measurements with a double proportional counter were made by Kramer (Kr-61, Kr-62). If the proper gas, pressure, and counter dimensions are chosen, the counter will detect the L and K x rays from the source with known efficiency, close to 100%. Observation of a K x ray then indicates the presence of a certain number of L-shell vacancies. Using a calculation similar to that outlined in Sec. 3.1, it can be shown that about 1.3 L-shell vacancies are produced for each K-shell vacancy. The observed L to K x-ray intensity ratio, corrected for this factor, thus is a direct measure of the L-shell fluorescence yield ω_{KL}.

A novel method of employing the proportional counter gas as an internal source was used by Curran *et al.* (Cu-49) and Godeau (Go-61) to measure ω_K of argon. Radiation of energy above the K edge of argon is directed into the counter (Godeau used 6-keV x rays from Fe^{55} source). This radiation is absorbed in the

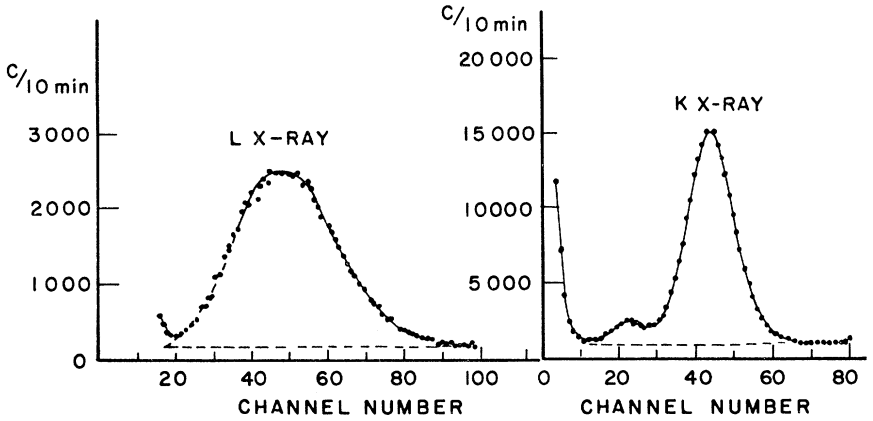

FIG. 4. The x-ray spectra of Pb^{203}, measured with a $1\frac{1}{2}$- $\times\frac{1}{4}$-in. NaI(Tl) scintillation detector are shown. The crystal was covered with a 0.001 - in. aluminum foil. These spectra were obtained by Persson and Sujkowski (Pe-61).

gas, and a large fraction of it photoionizes the argon K shell. With low enough pressure and small enough counter size, most of the argon K x rays emitted will escape from the counter, and only the escape peak will be observed (i.e., a peak corresponding to the energy of the incident radiation less the energy carried away by the escaping argon K x ray). However, if the vacancy in the argon K shell is filled by an Auger transition, there will be no K x ray emitted and the K-Auger electron will not escape. Therefore, a peak corresponding to the full energy of the incident radiation will be observed. Hence, the ratio of the counts in the escape peak to the counts in the full-energy photopeak, with small corrections for nonescaping K x rays, is a direct measure of ω_K for argon.

In the decay of pure electron capturing Cs^{131}, the mean L-fluorescence yield $\bar{\omega}_L$ of xenon has been measured from a determination of the relative L/K x-ray intensity ratio I_L/I_K with thin NaI(Tl) detectors (Ho-64) or proportional counters (Fi-55). Similar measurements have been made in the decay of Tl^{204} (Sc-57) and (Ra-65a). In these studies, the experimental or theoretical value of P_L/P_K, the ratio of probabilities for L and K capture, is required (RF-55, RF-60, Mo-63) together with the value of n_{KL}, the number of L vacancies produced in the filling of a K vacancy. The value of n_{KL} is found from the K Auger electron spectrum and total Auger electron intensity and has been given by RF-60, RF-55, and Li-60 (see Sec. 3.1). The mean L-fluorescence yield then is given by Eq. (21), with appropriate corrections for counting efficiencies of the L and K x rays.

A typical x-ray spectra observed using a proportional counter is shown in Fig. 3.

4.2.4. *Scintillation Counters*

Inorganic and organic scintillation detectors also have been widely employed in fluorescence yield measurements. Scintillation counters have some of the same advantages as the proportional counters. The NaI(Tl) crystals can be used to detect K x rays from elements with $Z \geq 20$ and L x rays emitted by elements with $Z \geq 50$. They also are very efficient in that all the x rays incident on the scintillator are counted.

In 1957, Roos (Ro-57) measured various K-shell fluorescence yields using a movable NaI(Tl) detector. Similar measurements were performed by Patronis, Braden, and Wyly (Pa-57) (using a proportional counter with variable solid angle). In this type of experiment, foils of the element under investigation were placed in a highly collimated flux of gamma radiation. The detector is placed such that the collimated radiation passing through the foil is incident on the detector. By moving the detector away from and toward the foil, the solid angle subtended by the detector can be varied. Since the fluorescent radiation from the foil is isotropic, the intensity of collimated radiation can be measured in the far position, and the sum of collimated radiation and the fluorescent radiation can be measured in the near position. Knowing the absorption of the primary radiation in the K shell gives the number of vacancies, and measuring the fluorescent radiation then gives the K-shell fluorescence yield.

In addition to their employment as simple x-ray detectors, scintillation counters also have found important applications in some of the more specialized experiments to be discussed in the following section.

Some typical x-ray spectra observed with NaI(Tl) scintillation detectors are shown in Fig. 4.

4.2.5. *Coincidence Methods*

The coincidence method has proved to be one of the more fruitful methods for investigation of atomic fluorescence yields. The principle has already been outlined in Sec. 2.3. The creation of a vacancy in an atomic shell may be accompanied by the emission of either a nuclear radiation or an x ray. If these accompanying radiations can be detected, they can be used to signal the creation of a vacancy in that shell. The coincidence counting rate between the accompanying radiation and the x rays produced in the filling of the vacancy is proportional to the fluorescence yield. Thus,

$$N_c = KN_{p_i}\omega_i, \tag{22}$$

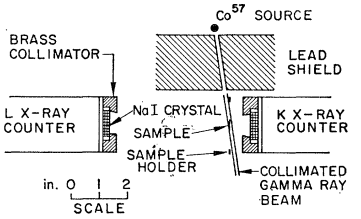

FIG. 5. The experimental arrangement used to measure ω_{KL} using the coincidence technique is shown. A thin sample is irradiated with a carefully collimated beam of 125-keV gammas from a Co^{57} source. These produce vacancies in the K shell. The resulting K and L x rays are counted by using two NaI(Tl) scintillation detectors connected so that the coincidence rate and the K and L x-ray counting rates can be determined.

where N_c is the observed coincidence rate, N_{p_i} is the number of radiations observed accompanying vacancies in the ith shell, and ω_i is the fluorescence yield of the ith shell. The constant K depends on the geometrical arrangement, the efficiency of the detector observing the ith shell radiations, and on the nature of the transition producing the vacancy in the ith shell.

Hagedoorn and Wapstra (Ha-60) first used this method to measure ω_K in Ti, Co, Cr, Zn, and Zr. Radioisotopes of these elements were used in this experiment, and a NaI(Tl) scintillation counter was used to detect the nuclear radiations which signaled the creation of a K-shell vacancy. A proportional counter was then used to observe the K x rays emitted in coincidence with the nuclear radiation.

Jopson *et al.* (Jo-61, Jo-63, Jo-64a, b, Jo-65) extended this method to measure L- and M-shell fluorescence yields. In Jo-61, radioisotopes were used to produce K-shell vacancies by electron capture processes, while in subsequent experiments, the K-shell vacancies were produced by photoionizing the K shell with an incident beam. In both cases, the coincidence rate between the K and L x rays was used to determine the mean L-fluorescence yield ω_{KL}. The K x rays were observed with thin NaI(Tl) scintillation detectors. Either scintillation or proportional counters were used to observe the L x rays, depending on the quantum energy of the x rays. The arrangement for these experiments is shown in Fig. 5. In Sec. 2.3, the method of measuring ω_3 separately was mentioned briefly. The experimental geometry for this experiment is shown in Fig. 6. Here, the K x-ray detector is shielded from the direct radiations of the target foil, and is surrounded by an annular radiator which views the target foil. This radiator is made of an element with the K edge between the energies of the K_{α_1} and K_{α_2} x rays coming from the target foil. Therefore, when K_{α_1} or K_β x rays strike the radiator, it reradiates its characteristic x rays into the x-ray detector. In this way, the K detector is triggered only by K_{α_1} or K_β x rays from the target and thus signals only vacancies in the L_3 or M, N, etc., shells. The coincidence rate between these events and the L x rays observed in the other counter thus depends only on ω_3.

Hohmuth *et al.* (Ho-63, Ho-64) measured L-fluorescence yields in Ru, Nb, Ag, Te, La, Ho, and Hg by taking coincidences between L and K x rays and between L x rays and gammas from radioisotope sources placed inside a proportional counter. The proportional counter detected the L x rays, while a scintillation counter was used to observe the K x rays outside the proportional counter.

Rao and Crasemann (Ra-65a) used the coincidence technique to measure ω_2 using a radioactive Tl^{204} source. In this experiment, NaI(Tl) scintillation detectors were used for the L and K x rays. The apparatus was then modified to measure the Coster–Kronig yield f_{23} in Hg. This modification involved the use of a proportional counter capable of resolving the L_{α_1} and L_{α_2} x rays of mercury from a thin Tl^{204} source (Ra-65b). In addition, the K x-ray detection system was modified with critical absorbers. Tungsten has its K edge between the K_{α_1} and K_{α_2} energies of mercury. By thus using a combination of tungsten, erbium, and tin, the K_{α_1} component of the Hg spectrum was substantially reduced in intensity, while the K_{α_2} component was retained. Coincidences were then taken between the K_{α_2} x rays and the L_{α_1} x rays. Since the K_{α_2} radiation indicates the occurrence of a $K-L_2$ transition and the L_{α_1} radiation indicates the filling of a vacancy in the L_3 subshell, the coincidence rate between K_{α_2} x rays and L_{α_1} x rays depend on the Coster–Kronig transition rate, f_{23}, for transfer of vacancies from the L_2 to the L_3 subshell. The quantitative relationships are

$$I_{L_3}/I_{L_2}=f_{23}(\omega_3/\omega_2) \tag{23}$$

$$\omega_2+f_{23}\omega_3=\nu_2=N_c/kN(K_{\alpha_2}) \tag{24}$$

$$\omega_{KL}=N_2\nu_2+N_3\omega_3=N_2(N_c/kN_{K\alpha 2})+N_3\omega_3, \tag{25}$$

where $k=\epsilon_L a_L \Omega_L$, the L x-ray detection efficiency, absorption factor, and geometry, respectively. These three equations (Ra-65b) can be solved to find f_{23}, ω_2, and ω_3, once the values of ν_2, I_{L_3}/I_{L_2} (the ratio of

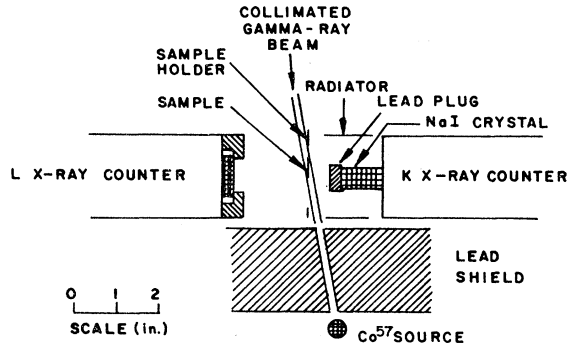

FIG. 6. The experimental arrangement used to measure ω_3 with the coincidence method is shown. This equipment is similar to that shown in Fig. 5, except that the K x-ray detector is modified to observe only the K x rays from the critical radiator. If the radiator is properly chosen, only K_{α_1} and K_β x-ray events in the target foil are counted. In this way, it is possible to isolate the L x rays due to vacancies in the L_3 subshell only.

L_3 to L_2 x rays emitted), and ω_{KL} have determined experimentally. In these equations, N_c = the number of coincidences counted between L_{α_1} and K_{α_2} x rays; $N(K_{\alpha_2})$ is the number of K_{α_2} x rays counted; and k is the detection efficiency for L x rays as defined above for the L x-ray counter.

It should be pointed out that the results of this experiment depend quite critically on knowing precisely the properties of the critical absorber used to eliminate the K_{α_1} component of the Hg K x-ray spectrum.

Halley and Engelkemeir (1-Ha-64) have measured high Z (Ra, Th, U, Pu, and Cm) L-fluorescence yields. Three methods were used. One involved counting the number of alphas emitted by a thin source and then calculating the fraction of these alphas, giving rise to L-shell vacancies. The L x rays were then counted and the fluorescence yield determined. This method also was used by Fink (Fi-57) to measure the mean L-fluorescence yield of bismuth $\bar{\omega}_L$ from Pb^{210} (RaD) decay (Ro-55). In this case, the L x rays from a carrier-free source of Pb^{210} were counted in a proportional counter, the number of L-shell vacancies being obtained from the counting of alphas from the Po^{210} daughter, in equilibrium with Pb^{210} parent through 4-day Bi^{210} (RaE). The alphas were counted with a very thin ZnS layer deposited on a photomultiplier tube. Very old (some years) sources of RaDEF had to be used to insure that the three isobars were in true radioactive equilibrium. Carrier-free sources were used to avoid spurious effects arising from fluorescent excitation from alpha and beta particles acting on solid sources (Fi-57). A second method (1-Ha-64) involved the coincidence method in which coincidences between L x rays and gammas were measured using NaI(Tl) detectors. In a third experiment (1-Ha-64), coincidences between L x rays detected in NaI(Tl) scintillation counters and alpha particles counted with solid-state detectors were determined.

Akalaev, Vartanov, and Samoilov (Ak-64) have measured $\bar{\omega}_L$ for Pu from a mixed source of $Cm^{242,244}$ and Eu^{154}, using the experimental relationship:

$$\bar{\omega}_L = (I_K/I_\gamma)(N_K/N_L)(1/\alpha_K),$$

where (I_K/I_γ) = ratio of Pu L x rays to 123-keV gamma of Eu^{154} decay. (N_K/N_L) = ratio of K x rays from Eu^{154} decay to the total L Auger electron intensity of Pu; and α_K = conversion coefficient of the 123-keV E2 gamma in Eu^{154} decay. The same authors (Ak-64) measured $\bar{\omega}_L = 0.66 \pm 0.08$ for Np from an Am^{241} source by measuring the L Auger electron spectra and its total intensity in a magnetic spectrometer, together with the intensity of the 60-keV E2 gamma from Am^{241} decay with NaI(Tl). From the L Auger electron spectrum, subshell Auger yields, $a_1 = 0.16 \pm 0.03$, $a_2 = 0.20 \pm 0.06$, and $a_3 = 0.43 \pm 0.09$ were found for Np ($Z = 93$), and assuming from Li-60 that $f_{12} = 0.10 \pm 0.04$, the Coster–Kronig yields f_{13} and f_{23} were evaluated. (See Table IV.) From the measured value of $\bar{\omega}_L$ and the Coster–Kronig and Auger subshell yields, the L-subshell fluorescence yields ω_1, ω_2, and ω_3 for $Z = 93$ also were found. (See Table III.)

4.2.6. High-Resolution Techniques

It has already been mentioned that the use of detectors with high resolution would substantially increase the scope of the experimental work in this field. In certain isolated cases, high-resolution detection methods have already been applied to good advantage. An interesting example of this is the determination of ω_2, f_{23}, and a_2 for plutonium by Salguero *et al.* (Sa-60). In this experiment, calculations of the L_2 subshell yields were computed from two sets of measurements, the coincidence rate between the L x rays and the alpha particles emitted by a Cm^{242} source, and the relative intensities of the L x-ray spectrum lines observed with a bent crystal spectrometer. The measured line intensities and available estimates of the Coster–Kronig yields f_{12} and f_{13} make it possible to compute the rate of vacancy creation per alpha decay in the L_2 subshell, and hence to evaluate the quantities ω_2, a_2, and f_{23} for that shell. This experiment can only be performed if strong radioactive sources (millicuries) are available, since the high-resolution bent crystal spectrometer has an efficiency much less than one percent. Correction for the variation in reflectivity with x-ray wavelength of the bent crystal must be made in this work. Careful measurements of the reflectivity variation have been reported by Cochran and Ross (Co-58) and Knowles (Kn-64).

A recent development of great promise is that of lithium-drifted silicon and germanium detectors suitable for low-energy x-ray spectrometry. Such detectors can be fabricated essentially windowless (i.e., with no dead layer) and used to observe x rays of energies down to a few keV with excellent resolution. For example, a Si(Li) detector operated at liquid-nitrogen temperature (77°K) in combination with a low-noise FET preamplifier whose input field-effect transistor is mounted next to the detector and cooled to 77°K can be optimized to achieve a resolution for the K_α x-ray group of better than 740-eV FWHM. This is adequate to resolve the K_β x-ray group from the K_α group for all elements of atomic number greater than $Z = 32$ (germanium). This can be seen in Fig. 7, which displays the characteristic K x rays of iron, germanium, and zirconium taken with such a cooled Si(Li) detector system having an active area of 110 mm² and a 3-mm sensitive depth. The spectra were taken through a 0.010-in. beryllium window. Similar spectra also have been obtained with windowless lithium-drifted germanium detectors. One interesting application of Si(Li) and Ge(Li) x-ray detectors would be to measure the fluorescence yields of the M shell in several elements by taking the coincidence rate between the K_β-series x rays, which mark vacancies in the M shell, and M x rays.

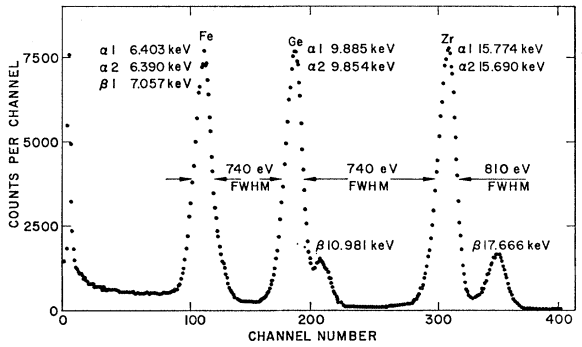

FIG. 7. Characteristic K x-ray spectra of iron, germanium, and zirconium taken with a 110 mm²×3 mm lithium-drifted silicon detector cooled to 77°K connected to a FET preamplifier whose input field-effect transistor also was cooled to 77°K. Typical resolution for the K_α x-ray group is about 740-eV FWHM. The K_β x-ray group is clearly separated for elements with atomic number above germanium ($Z=32$). This spectrum was furnished by D. Grunau of Technical Measurements Corporation. Similar spectra have also been obtained with windowless lithium-drifted germanium detectors.

Another potentially important new device which could be employed for fluorescence yield measurements is the high-current (≈10 mA), low-energy (≈500 keV) ion accelerator, already mentioned in Sec. 2.2. Using intense proton or alpha-particle beams to excite primary vacancies, it is possible that high-resolution detectors and coincidence methods could be employed to great advantage in determining more precisely the fluorescence yields of higher atomic shells. For this work, it would be highly desirable to have available more precise calculations of the atomic ionization cross sections of heavy charged particles.

5. EXPERIMENTAL RESULTS AND COMPARISON WITH THEORY

5.1. *K*-Shell Fluorescence Yields

The earliest theoretical calculations of the Auger fluorescence yield ω_K are due to Wentzel (We-27), who took into account only the L-shell participation in the Auger process:

$$\omega_K=(1+a/Z^4)^{-1}, \quad \text{where} \quad a=\approx 10^6. \tag{26}$$

More detailed calculations were made by Burhop (Bu-35) and by Pincherle (Pi-35) using nonrelativistic theory, and by Massey and Burhop (Ma-36) using a relativistic theory. Hydrogen-like single-electron wave functions with Slater screening were used. Account is taken of transitions involving M and N shells in the Auger process if the following values of the parameter a are used: (Bu-52) $a=9\times10^5$ for $Z<10$; $a=1.19\times10^6$ for $10\leq Z\leq 18$; and $a=1.27\times10^6$ for $Z>18$. These theoretical calculations corroborated Eq. (26), according to which the values of ω_K should be independent of the frequency of the exciting radiation, or of the manner in which K-shell vacancies are created. Comparison with experiment has fully substantiated this expectation (Bu-52), based on our present understanding of the Auger processes.

Rubinstein and Snyder (Ru-55) used the Hartree self-consistent field method of computing the initial wave functions for argon, krypton, and silver. Higher values of ω_K were obtained, in better agreement with experiment, particularly in the case of argon, for which their calculation gives $\omega_K=0.13$, rather than 0.08 according to Burhop (Bu-52). The approximations used, however, in particular the central field polynomial, are likely to lead to larger errors for low Z elements, so that the disagreement with the earlier calculations at low Z may not be significant.

Attempts have been made to fit a semiempirical formula of the type

$$\omega_K=[1+a(Z-b-cZ^3)^{-4}]^{-1}, \tag{27}$$

which can be written in the more usual alternate form

$$[\omega_K/(1-\omega_K)]^{-4}=-A+BZ+CZ^3, \tag{28}$$

to the experimental results (Bu-55, La-56a, Li-60). The term involving the constant A essentially is a correction for screening, while the term involving CZ^3 carries the relativistic correction. The latter is negligible at low Z; on the other hand, the screening factor is very important at low Z, but it is difficult to determine it accurately, since its effect is small for medium- and high Z, where the experimental measurements are more accurate. Thus, Eqs. (27) and (28) introduce a considerable error when extrapolated to low Z ($Z<18$). These early theories assumed, moreover, that all of the electrons involved lie in discrete energy states, as in a gaseous atom, but this in fact is not true for low Z elements, in which the L electrons lie in the valance band and have wave functions which depend on the structure of the solid.

Furthermore, no allowance is made for the fact that the L- and M shells below $Z=18$ are incomplete. For ω_K values below $Z=18$, Achard (Ac-60) has shown that the theory of K-shell ionization by electron impact predicts the correct variation of K x-ray yields down to boron ($Z=5$), provided that Eq. (26) (Bu-52), rather than Eq. (27) or (28), is used for ω_K. The only serious disagreement between theory and experiment then remaining at very low Z is for beryllium ($Z=4$), where the observed K x-ray yield is only about half that predicted (Cam-63). Although considerable systematic error could be present in the beryllium experiments, the likely explanation of the disagreement is a breakdown of the formula for ω_K.

The constants A, B, and C in Eq. (28) are obtained from experiment by least-squares analysis. Curves of Eq. (27) or (28), together with available experimental points, have been published by many authors (Wa-59, Gr-56, Be-55, La-56a, Br-53, Bu-55, Bu-52, and Ro-57). Listengarten (Li-60) has compared available ω_K values

with Eq. (28) using values of constants A, B, and C from the literature, as shown in Table I. As Listengarten (Li-60) has observed, the curves of Li-56a and Wa-59 are rather similar, in agreement with available experimental data. In the region $23 \leq Z \leq 57$, the two curves are rather close, within 10% at the edges of the region, and giving the same value of ω_K for $Z \approx 40-45$.

Taylor and Merritt (Ta-63) have recently reported a new set of precision ω_K measurements for V, Cr, and Cu, using radioactive electron-capture sources of Cr^{51}, Mn^{54}, and Zn^{65}, respectively. Account was taken of the ratios of K/total capture and of capture from higher shells. Corrections for electron exchange effects were applied as given by Bahcall (Ba-63), which resolve the discrepancy previously noted between measured allowed L/K-capture ratios and their theoretical values (RF-55, RF-60, Mo-63). Since the ω_K values of Ta-63 are based on absolute measurements of disintegration rates and K x-ray emission rates, they are not subject to errors arising from self-absorption-scattering of low-energy Auger electrons in the solid sources or from quantitative measurement of Auger electron intensities. Likewise, the difficulties of resolving electron or K x-ray peaks or of determining detector efficiencies as a function of energy are avoided. The largest corrections are for capture from higher shells and for K x rays stopped in the Auger electron absorbers. The latter correction was directly measured and was kept small ($\sim 3\%$). Reproducibility of the results was 0.2% or better. The quoted errors of $\pm 2\%$ (Table II) include allowances for possible systematic errors, corrections, and capture ratios. The ω_K values of Ta-63 are significantly larger than previously accepted experimental values (Table II) in the region $24 \leq Z \leq 29$, as well as larger than Callan's theoretical values (Ca-63b) in this region, but not as large as the earlier theoretical estimates of Rubenstein and Snyder (Ru-55).

Listengarten (Li-62) has carried out new calculations of the probability of the Auger effect for elements with $Z=65$, 81, and 92. Previous nonrelativistic calculations of the relative intensities of the K-LL series of Auger lines (from which values of ω_K are computed) disagreed with experiment by some 30–40% for medium Z and by some 400% for $Z>81$. The relativistic calculations of Massey and Burhop (Ma-36) did not remove the disagreement in the K-LL Auger intensities. Recently, Asaad (As-59, As-65) gave results for relativistic calculations for $Z=80$, the screening being taken into account by means of nonrelativistic self-consistent Hartree field.

In Listengarten's calculations (Li-62), more accurate relativistic expressions (in jj coupling) for the probability of the various K-LL Auger transitions were obtained from general electrodynamic quantum theory. Screening was taken into account through the use of the Thomas–Fermi–Dirac statistical model. These results show that the total probability for K-LL Auger transitions is more than twice as large as the corresponding nonrelativistic value, the greatest increase being in the probabilities for K-L_1L_1 and K-L_1L_2 Auger transitions. The probability of an Auger transition involving only the p-electrons is essentially unchanged, but the relative contribution from the K-L_2L_2, K-L_2L_3, and K-L_3L_3 transitions is significantly reduced, which is in good agreement with experiment.

TABLE I. Values of empirical constants in Eq. (2a) from various authors (Cf. Li-60).

Constants	Bu-52	La-56a	Wa-59
$A\times 10^2$	4.4	2.17	6.4
$B\times 10^2$	3.46	3.318	3.4
$C\times 10^6$	1.35	1.14	1.03

To evaluate the K-fluorescence yield ω_K a knowledge of the total width of the K level is required, together with the value of the radiation width of the K level, since $\omega_K=\Gamma_{X_K}/\Gamma_{T_K}$. Using the ratio of Auger electron intensities

$$[(K-LX)+(K-XY)]/(K-LL),$$

where the numerator is obtained from experiment (Cf. Li-60) and the denominator from the theoretical total K-LL Auger probability (Li-62), the total width of the K level can be found; as given by Listengarten, $\Gamma_{T_K}=2.07$ eV for $Z=65$; 2.52 eV for $Z=81$; and 4.16 eV for $Z=92$.

The radiation width of the K level for emission of K_α x rays can be obtained from the K-$L_{2,3}$ Auger transition probability for $Z=80$ calculated by Asaad (As-59, Aa-65), $\Gamma_{X_K}=49.6$ eV at $Z=80$. Evaluation of Γ_{X_K} for other values of Z between 51 and 92 is done by means of the calculations of Massey and Burhop (Ma-36), which give a Z^4 dependence of the K-$L_{2,3}$ (the K_α transition) probability. The ratio of $K_\alpha/K_{\text{total}}$ x-ray quanta in these calculations was obtained from Wa-59. Although the absolute values from Massey and Burhop (Ma-36) are too low, owing to their use of Slater screening constants, the relative Z^4 dependence can be accepted as approximately correct. From this method, Listengarten (Li-62) has computed theoretical values of $\Gamma_{X_K}=20$ eV at $Z=65$; 49 eV at $Z=81$; and 81.5 eV at $Z=92$. Extrapolating for other values of Z in the region $Z=65$ to 93, Listengarten has evaluated values of the K-fluorescence yield from $\omega_K=\Gamma_{X_K}/\Gamma_{T_K}$, and these are given in Table II, and are used in Fig. 8 to construct the theoretical curve in this region of atomic number.

Comparison of these results with experiment (Table II and Fig. 8) shows that the agreement with experimental data is better at high Z for Listengarten's relativistic calculations than for the older nonrelativistic results, the best agreement coming in the heavy element region $Z=92-94$, for which no previous relativistic calculations exist.

TABLE II. Summary of K-fluorescence yields and comparison with theory.[a]

Z	Element	ω_K(experimental)	Ref.	ω_K(theory)	Ref.
6	C	0.0009	Br-53		
7	N	0.0015	Br-53		
8	O	0.0022	Br-53		
10	Ne	0.0081	Br-53		
		0.043±0.004	Fr-58		
12	Mg	0.0280±0.011	Ko-64		
		0.013	Br-53		
		0.008±0.003	Ri-59		
13	Al	0.008±0.003	Fr-58		
		0.0381±0.015	Ko-64		
		0.045±0.002	Be-59		
14	Si	0.038	Br-53		
16	S	0.083	Br-53	0.098	Ca-63b
17	Cl	0.093±0.003	Be-59	0.117	Ca-63b
		0.108	Br-53		
18	Ar	0.081±0.006	1-Ha-55	0.138	Ca-63b
		0.087±0.007	Go-61	0.13	Ru-55
		0.123	Br-53		
		0.129±0.011	He-55		
		0.140±0.0014	Wa-62		
19	K			0.155	Ca-63b
20	Ca	0.15	Br-53	0.165	Ca-63b
		0.207	La-34		
22	Ti	0.180±0.010	Ha-57	0.213	Ca-63b
			Ha-60		
		0.22	Ru-62		
23	V	0.24	Ru-62		
		0.253±0.005	Ta-63		
		0.305±0.027	Fr-58	0.242	Ca-63b
		0.23±0.02	Ko-61		
24	Cr	0.26	Ru-62		
		0.222±0.003	Kr-62	0.272	Ca-63b
			Kr-61		
		0.277±0.042	Ba-65		
			Le-65		
		0.264 (av)	Br-53		
		0.219±0.012	Ha-60		
		0.20±0.03	2-Mo-61		
		0.285±0.006	Ta-63		
25	Mn	0.273±0.003	Kr-62	0.291	Ca-63b
			Kr-61		
		0.28	Ru-62		
		0.308±0.015	Fr-58		
		0.27±0.02	Ko-61		
		0.33±0.03	2-Mo-61		
26	Fe	0.308±0.015	Ro-57	0.319	Ca-63b
		0.375	Br-53		
		0.314	Br-53		
		0.32	Br-53		
		0.343	La-34		
27	Co	0.310±0.010	Ko-58a	0.346	Ca-63b
			Ko-58b		
			Ha-60		
			Ha-57		
28	Ni	0.366±0.011	Ro-57	0.378	Ca-63b
		0.38±0.01	Be-59		
		0.33±0.02	Pa-57		
		0.385	Br-53		
		0.374	Br-53		
		0.436	La-34		
29	Cu	0.400±0.004	Kr-61	0.407	Ca-63b
			Kr-62		
		0.42±0.02	Ko-61		
		0.410±0.012	Ro-57		
		0.454±0.009	Ta-63		
		0.390±0.020	1-Ha-55		
			Pa-57		
		0.419	Br-53		
30	Zn	0.446±0.012	Ro-57	0.438	Ca-63b
		0.440±0.020	Pa-57		
		0.430±0.020	Ha-60		
		0.440	Br-53		
		0.476	La-34		

TABLE II (*Continued*)

Z	Element	ω_K(experimental)	Ref.	ω_K(theory)	Ref.
31	Ga	0.427±0.004	Kr-61	0.469	Ca-63b
			Kr-62		
		0.47±0.02	Ko-61		
		0.53±0.03	Dr-57		
32	Ge			0.510	Ca-63b
33	As	0.53	Br-53	0.548	Ca-63b
34	Se	0.575	St-37	0.585	Ca-63b
		0.578	Br-53		
		0.547	Br-53		
		0.585	La-34		
35	Br	0.565	Br-53	0.628	Ca-63b
		0.623 (av)	Br-53		
36	Kr	0.620±0.030	We-55	0.660	Ca-63b
		0.660±0.020	He-55	0.67	Ru-55
		0.67	Br-53		
37	Rb			0.680	Ca-63b
38	Sr	0.640±0.030	Ha-60	0.702	Ca-63b
		0.644	Br-53		
39	Y			0.719	Ca-63b
40	Zr	0.700±0.020	Ro-57	0.737	Ca-63b
		0.69	St-37		
		0.645	Gr-56		
41	Nb	0.730±0.020	Ro-57	0.754	Ca-63b
		0.713	Gr-56		
42	Mo	0.730±0.020	Ro-57	0.770	Ca-63b
		0.714	Gr-56		
		0.785	Br-53		
		0.735	St-37		
		0.765 (av)	Br-53		
43	Tc	0.697(+0.060, −0.046)	Ra-61	0.785	Ca-63b
		0.700±0.030	La-56a, b		
44	Ru			0.799	Ca-63b
45	Rh	0.786±0.015	Ro-57	0.812	Ca-63b
		0.801	Br-53		
		0.779	Gr-56		
		0.77	St-37		
46	Pd	0.790±0.015	Ro-57	0.822	Ca-63b
		0.835	Br-53		
		0.781	Gr-56		
47	Ag	0.821±0.019	Ro-57	0.833	Ca-63b
		0.840 (av)	Br-53	0.85	Ru-55
		0.81	St-37		
		0.813	Gr-56		
48	Cd	0.827±0.015	Ro-57	0.843	Ca-63b
		0.846	Br-53		
		0.819	Gr-56		
		0.773 (av)	Br-53		
49	In	0.820±0.020	1-Ha-55		
		0.87±0.03	La-56a, b		
50	Sn	0.846±0.012	Ro-57		
		0.836±0.013	Fa-57		
		0.840	Gr-56		
		0.855	Br-53		
		0.81	St-37		
51	Sb	0.862	Br-53		
52	Te	0.872	Br-53		
53	I	0.91±0.03	Fo-59		
		0.88	Br-53		
54	Xe	0.880±0.030	He-55	0.872	Ca-63b
		0.81	Br-53		
55	Cs	0.873±0.015	Er-61		
		0.898±0.002	Gr-61b		
		0.890	Br-53		
56	Ba	0.870±0.007	Br-53		
		0.85	Gr-56		
57	La	0.88±0.01	Ke-56		
		0.94	Gr-56		
58	Ce	0.90	Gr-56		
59	Pr				
59	Pr	0.88	Br-53		
63	Eu	0.908±0.007	Su-62		

TABLE II (*Continued*)

Z	Element	ω_K(experimental)	Ref.	ω_K(theory)	Ref.
64	Gd	0.925±0.005	1-Mo-61		
65	Tb			0.924	Li-62
66	Dy	0.943±0.007	Gr-61a		
67	Ho			0.930	Li-62
68	Er	0.955±0.022	Br-59		
69	Tm			0.936	Li-62
70	Yb	0.936±0.010	Gr-56		
71	Lu			0.941	Li-62
73	Ta			0.946	Li-62
74	W			0.945	Ca-63b
75	Re			0.951	Li-62
77	Ir			0.956	Li-62
78	Pt	0.942	Br-53		
79	Au			0.960	Li-62
				0.953	Ca-63b
80	Hg	0.952±0.003	Na-60	0.961	Li-62
		0.946±0.008	Br-53	0.955	Ca-63b
81	Tl			0.962	Li-62
82	Pb	0.96	Gr-56	0.963	Li-62
83	Bi	0.96	Gr-56	0.963	Li-62
		0.934	Br-53	0.958	Ca-63b
		0.976	Br-53		
84	Po	0.944±0.008	Gr-56	0.963	Li-62
		0.894	Br-53		
90	Th			0.963	Li-62
91	Pa			0.963	Li-62
92	U	0.967±0.010	Gr-56	0.963	Li-62
93	Np	0.938±0.010	Ho-58	0.963	Li-62

[a] Most values before review of Gr-56 and Br-53 are referred to in those summaries, respectively. This accounts for different values with same reference number. (Cloud chamber and approximate results have not been included.)

Callan (Ca-63b) has computed radiation and Auger level widths for K levels in the region of $16 \leq Z \leq 83$. The former were computed empirically from the quasi-hydrogenic approximation

$$\Gamma_{X_K} = \sum_n A_n Z^4, \tag{29}$$

where the empirical coefficients A_n are averaged values of the $1s$-np dipole transition probabilities. The approximation was used of multiplying the A_n coefficient for a full shell by the fraction of electrons in the shell, which accounts adequately for the fraction of the widths due to an unfilled shell. The Auger widths, Γ_{a_K} (from which the total width $\Gamma_{T_K} = \Gamma_{X_K} + \Gamma_{a_K}$) were computed from K-LL widths corrected both for $(K\text{-}XY)/(K\text{-}LL)$ ratios from Geffrion and Nadeau (Ge-59) and for relativistic effects for heavy elements.

The results for Γ_{X_K} and $\Gamma_{T_K} = \Gamma_{X_K} + \Gamma_{a_K}$ agree within 5% for all but the lightest elements with those given by Parratt (Pa-59); for the lightest elements, the differences in Γ_{T_K} are less than 0.15 eV.

The K-shell fluorescence yields from

$$\omega_K = \Gamma_{X_K}/(\Gamma_{X_K} + \Gamma_{a_K})$$

thus were computed by Callan in the region $Z = 16-83$. They agree well with the theoretical results of Listengarten (Li-62), as seen in Table II and Fig. 8, for the high-Z region. When compared to curves based on Eq. (28), Callan's results lie slightly higher than those of Wa-59 and Bu-55 in the middle-Z region. From $Z = 40$ to 50, Callan's results also tend to be higher than the values of Roos (Ro-57), which may be the result of neglect of the relativistic increase in the Auger yield in this region. However, the maximum deviation does not exceed about 0.04 from the experimental values in the middle-Z region, and one concludes that the use of screened hydrogenic-type approximations is reasonably well justified for both Γ_{X_K} and Γ_{a_K} widths for the K shell. Callan's values are shown in Table II, and they are used to construct the theoretical curve in the middle-Z region shown in Fig. 8.

The K-fluorescence yield can be measured experimentally if the fraction of the total number of orbital electron capture events by a radioactive nuclide which produce a K-shell vacancy is known, since one can determine the ratio of the rate of K x-ray emission to the total electron capture rate (see Ta-63). However, to calculate theoretically the fraction of the total electron capture events producing a K-shell vacancy, one must correct for the effect of electron exchange and imperfect atomic overlap according to Bahcall (Ba-63)

$$\lambda_K/\lambda_{\text{total}} = (\lambda_K/\lambda_{\text{total}})^0 \, B_K, \tag{30}$$

where $(\lambda_K/\lambda_{\text{total}})^0$ is the usual theoretical ratio of the probability of K capture to the total electron capture probability (Br-58), and B_K is the exchange correction factor defined by Bahcall as

$$B_K = |f(1s')/\psi(1s)(0)|^2, \tag{31}$$

where $f_{(1s')}$ is the amplitude for the production of a vacancy in the K shell of the *daughter* atom, and $\psi(1s)(0)$ is the one-electron K-shell wave function,

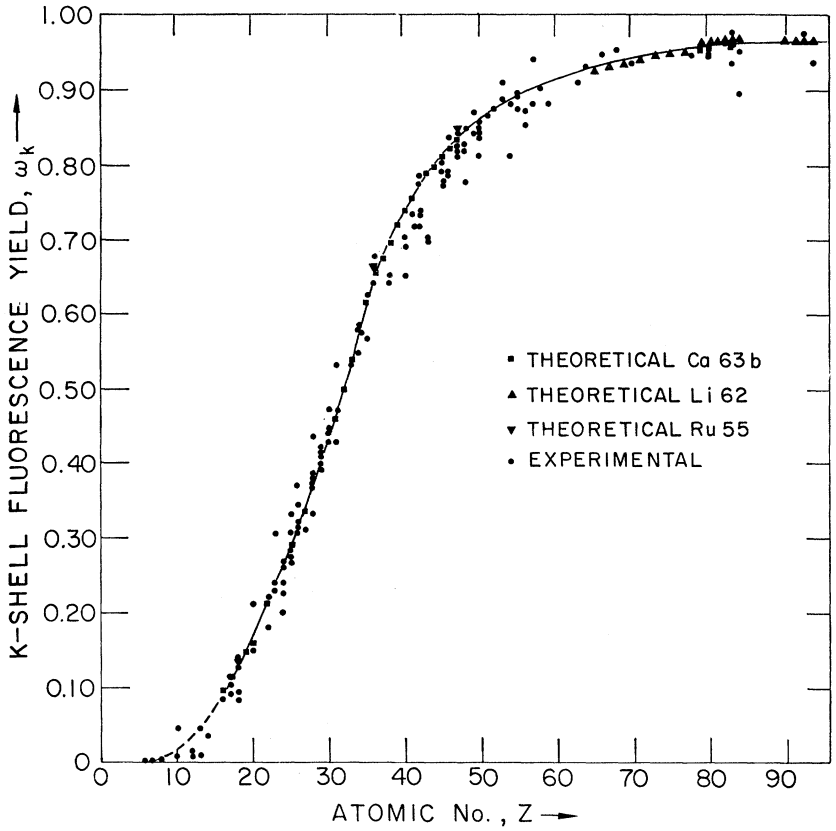

FIG. 8. The K-shell fluorescence yields are shown as a function of atomic number. The closed circles represent experimental values. The theoretical values from three different calculations are shown. The solid curve is the "best fit" theoretical curve.

evaluated at the nucleus, of electrons in the *initial* atom. Numerical values of B_K have been computed by Bahcall (Ba-63) using the analytic Hartree–Fock wave functions of Watson and Freeman (Wa-61) in the region limited to $14 \leq Z \leq 37$. These values of B_K are given by the formula

$$B_K = 1 - 0.929/Z + 20.98/Z^2 - 316.5/Z^3,$$

for

$$14 \leq Z \leq 37. \tag{32}$$

The exchange correction is accurate to within about 2%.

All available theoretical and experimental values of ω_K are gathered in Table II and exhibited in Fig. 8. Experimental ω_K values before the summary of Broyles, Thomas, and Haynes (Br-53) are taken or averaged from these authors for elements for which no other data exists, except that no result based on the unreliable cloud chamber method has been included. Similarly, the summary of ω_K values of Gray (Gr-56) was used to obtain more recent experimental values appearing since Br-53. All other experimental data were collected from the literature through 10 May 1966.

Those values of ω_K which were measured by means of the more accurate experimental techniques discussed above appear to agree best with the theoretical curve, Fig. 8, which has been drawn from the theoretical results of Callan (Ca-63b) and Listengarten (Li-62). When one requires a value of the K-fluorescence yield for other purposes, a suitable procedure would be to take the value from the curve, Fig. 8, especially in cases where a variety of experimental points is offered.

5.2. *L*-Shell Fluorescence and Coster–Kronig Yields

An early attempt to compute theoretical values of mean L-shell fluorescence yields was made by Pincherle (Pi-35). He employed nonrelativistic, hydrogen-like wave functions with Slater screening. These results do not agree satisfactorily with experimental results (Bu-52). A recent theoretical calculation of the Auger effect in the L shell (As-65) has been performed. The only other theoretical work which bears on L-shell fluorescence yields is that of Massey and Burhop (Ma-36) who have given theoretical values of Γ_{X_i} for the L subshells; see Eqs. (13) and (14). As stated in Ref. Li-60, these values are too small. The probable reason for this circumstance is that Slater screening was used rather than more accurate atomic wave functions. Listengarten (Li-60) has generated semitheoretical curves for the fluorescence and Coster–Kronig yields of the L subshells. These are shown as curves in Figs. 9, 10, and 11 on which experimental points are also shown for comparison.

The Listengarten curves were constructed in a manner similar to that of Kinsey (Ki-48a). Radiation,

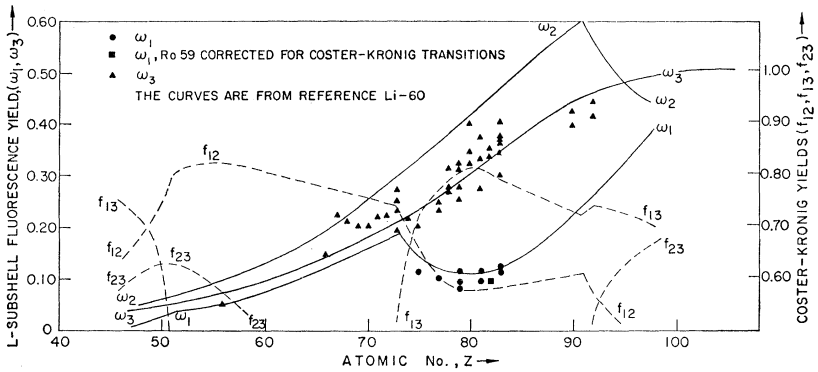

FIG. 9. The values of ω_1 and ω_3 are shown, together with the semi-theoretical estimates of Listengarten (Li-60) in the form of the curves.

Auger, and Coster–Kronig widths were chosen in the region $Z=47$ to 98. The method differs from Kinsey's in the following ways:

(a) The curves are normalized to experimental data at $Z=47$, 54, 55, 56, and 82 (see Li-60);

(b) The Auger widths Γ_{a_i} were assumed not to be constant but were increased linearly from $Z=47$ to 82 and even more rapidly for $Z\geq 82$;

(c) The Massey–Burhop (Ma-36) radiation widths, Γ_{X_i}, were increased by 40%, 20%, and 10% for $Z=51$, 79, and 92, respectively;

(d) Use was made of the fact that the Coster–Kronig width Γ_{ik} changes sharply at $Z=51$, 73, 91, and 92. For other regions of Z, the Γ_{ik} values obtained for $Z=55$ and 82 were then extrapolated continuously with Z in accordance with Coster–Kronig electron energies. It was further assumed that $L_2 \rightarrow L_3M_{4,5}$ transitions cause Γ_{23} to increase for $Z\geq 91$ in the same way as Γ_{13} increases for $Z\geq 73$.

In Fig. 9, which shows Listengarten's curves, experimental values for ω_1 and ω_3 have been entered. Figure 10 shows the Listengarten curves and the experimental points for ω_2. In these figures, the experimental values for ω_1 and ω_2 reported by Küstner and Arends (Kü-35) and Roos (Ro-59) shown in Table III are not entered because:

(a) In the case of ω_1, the results do not take into account Coster–Kronig transitions ($L_1 \rightarrow L_{2,3}$), the correction for which introduces even more uncertainty than exists in the original data;

(b) In the case of ω_1 values obtained by Kinsey (Ki-48b), the L x-ray transitions ascribed to the L_1 subshell had to be measured with the aid of critical absorbers, a method which involves considerable uncertainty. In addition, the decay schemes of Pb^{210}(RaD) and Bi^{212}(ThC) on which assumptions were based were not correctly established at the time;

(c) In the case of ω_2, the critical absorption method is not sufficiently precise to permit an accurate separation into ω_2 and ω_3 values. Moreover, the ratio of subshell vacancies $N_2:N_3$ must be calculated from photoelectric cross sections, a procedure involving some inaccuracies;

(d) The ω_2 value for $Z=79$ of Päschke (Pä-63) depends on assuming a value for f_{23} and is therefore not entered. Similarly, the ω_3 value which depends on assumed values for f_{12}, f_{13}, and f_{23} is omitted. On the other hand, Päschke's value for ω_1, determined by analyzing the Auger electrons and the L x rays, depends on a calculated subshell vacancy ratio of $N_1:N_2:N_3=1:1:2$ for excitation by electron bombardment, but not on the assumption of values of Coster–Kronig yields, and so it is retained on the plot.

The ω_1 points retained in Fig. 9 were measured by various methods based on Auger electron intensity measurements with high resolution beta spectrometry (Pä-63, Su-61a), or by the measurement of radiation widths according to Kinsey (Ki-48b).

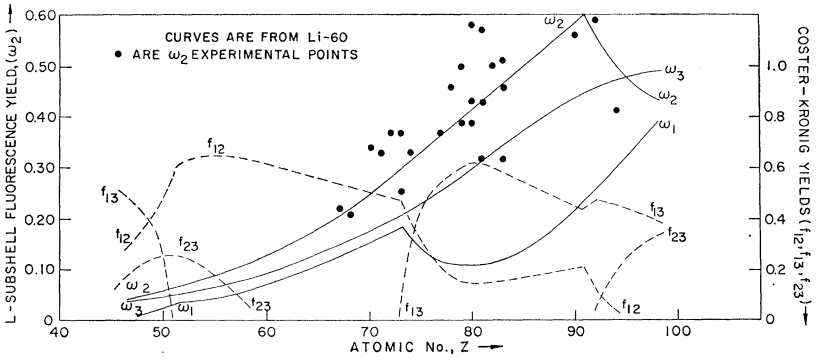

FIG. 10. The values of ω_2 are shown, together with the semi-theoretical estimates of Listengarten (Li-60) in the form of the curves.

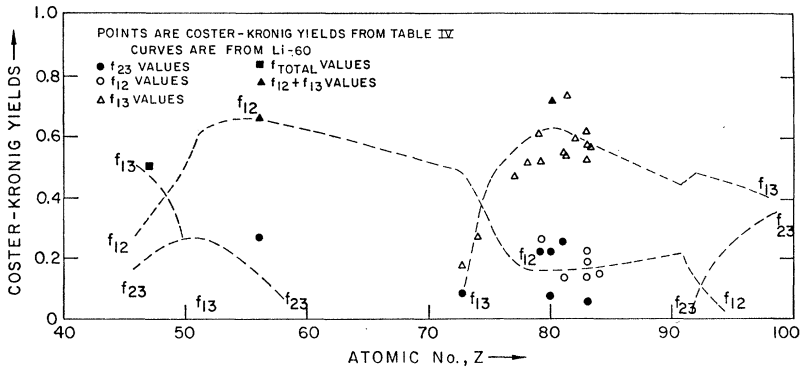

FIG. 11. This figure shows the available values of L shell Coster–Kronig yields compared with the semi-theoretical estimates of Listengarten (Li-60) in the form of the curves.

TABLE III. Experimental values of L-subshell fluorescence yields.

Z	Element	ω_1	ω_2	ω_3	Ref.
56	Ba			0.05±0.01	Bu-58
66	Dy			0.145±0.055	Zi-63
67	Ho		0.22±0.04	0.22±0.03	Jo-64a
68	Er		0.21±0.04	0.21±0.03	Jo-64a
70	Yb		0.34±0.05	0.20±0.02	Jo-64a
71	Lu		0.33±0.06	0.22±0.03	Jo-64a
72	Hf		0.37±0.06	0.22±0.03	Jo-64a
73	Ta	0.28±0.07	0.23±0.04	0.23±0.02	Ro-59
			0.25±0.02	0.27±0.01	Ra-65
	Ta	0.284[a]	0.326[a]	0.191[a]	Kü-35[a]
	Ta		0.37±0.06	0.25±0.03	Jo-64a
74	W	0.305[a]	0.311[a]	0.207[a]	Kü-35
	W		0.33		Ki-48
75	Re	0.11		0.20	Ki-48
77	Ir	0.370[a]	0.281[a]	0.244[a]	Kü-35[a]
	Ir	0.10	0.37	0.23	Ki-48
78	Pt	0.35±0.08	0.31±0.04	0.275±0.03	Ro-59
	Pt	0.392[a]	0.274[a]	0.262[a]	Kü-35[a]
	Pt		0.46±0.07	0.31±0.04	Jo-64a
79	Au	0.08±0.01	0.26±0.03	0.24±0.02	Pä-63
	Au	0.410[a]	0.272[a]	0.276[a]	Kü-35[a]
	Au	0.09	0.39	0.25	Ki-48
			0.343±0.007		La-65
	Au	0.36±0.09	0.27±0.04	0.32±0.03	Ro-59
	Au		0.50±0.08	0.31±0.04	Jo-64a
80	Hg		0.433±0.090	0.342±0.010	2-Ha-55
			0.39±0.03	0.40±0.02	Ra-65a
	Hg		0.58±0.10	0.32±0.05	Jo-64a
81	Tl	0.09	0.43	0.27	Ki-48
	Tl			0.33±0.02	Wi-58
	Tl	0.11±0.025	0.32±0.05		Su-61a
	Tl		0.57±0.10	0.37±0.06	Jo-64a
82	Pb	0.475[a]	0.264[a]	0.337[a]	Kü-35[a]
	Pb	0.37±0.04	0.24±0.04	0.35±0.04	Ro-59
	Pb		0.50±0.08	0.35±0.05	Jo-64a
83	Bi	0.11[b]	0.32[b]	0.34[b]	To-58[b]
	Bi	0.487[a]	0.255[a]	0.367[a]	Kü-35
	Bi		0.46	0.30	Ki-48
	Bi			0.36	Ri-60
	Bi		0.51±0.08	0.37±0.05	Jo-64a
	Bi	0.12±0.01	0.32±0.04	0.40±0.05	Ro-55
90	Th		0.56	0.39	Ki-48
	Th			0.42	2-Ha-55
92	U		0.59	0.41	Ki-48
	U			0.44	St-37
93	Np	0.19±0.04[c]	0.78±0.19[c]	0.57±0.12[c]	Ak-64
94	Pu		0.413±0.02		Sa-61

[a] Uncorrected for Coster–Kronig transitions.
[b] Assuming $f_{23}=0$. This assumption is also made for all ω_2 values given in Jo-64a.
[c] Assuming from Li-60 that $f_{12}=0.10\pm0.04$.

TABLE IV. Summary of experimental L-shell Coster–Kronig yields.

Z	Element	f_{12}	f_{13}	f_{23}	$f_{12}+f_{13}$	f_{total}	Reference
47	Ag					≈0.5	Bu-52
56	Ba			0.26±0.26	0.66±0.07		Bu-58
73	Ta		0.19±0.20				Fe-65
73	Ta			0.20±0.04			Ra-65a
74	W		0.27±0.03				Fe-65
77	Ir		0.46±0.06				Fe-65
78	Pt		0.50±0.05				Fe-65
79	Au	0.25±0.13	0.51±0.13	0.22±0.07[a]			Pä-63
79	Au		0.61±0.07				Fe-65
80	Hg			≤0.13			Ra-64
80	Hg			0.22±0.04	0.74±0.04		Na-60
80	Hg			0.08±0.02			Ra-65a
81	Tl		0.76±0.10				Fe-65
81	Tl		0.57±0.10				Pe-61
81	Tl	0.17±0.05	0.56±0.07	0.25±0.13		0.73[a]	Su-61a
81–83		0.24	0.52	0[a]			Bu-56
82	Pb	0.16	0.60	0[a]	(calculated from Ki-48b)		Li-60
83	Bi	0.16	0.62	0[a]			To-58
83	Bi	0.19±0.05	0.58±0.05	0.06(+0.14, −0.06)			Ro-55
83	Bi	0.19	0.58	0([a])			Ri-58
93	Np	0.10±0.04[a]	0.55±0.09	0.02±0.05			Ak-64

[a] Assumed in order to obtain the other values.

Table IV shows a summary of experimental L-shell Coster–Kronig yields. These are plotted in Fig. 11, together with the semitheoretical curves of Listengarten (Li-60).

Table V lists experimental values of ω_{KL} and some mean L-fluorescence yields, $\bar{\omega}_L$, measured by various methods. Figure 12 shows ω_{KL} as a function of Z, and Fig. 13 shows $\bar{\omega}_L$ vs Z. In Figs. 12 and 13, measurements based on photoexcitation are shown as solid points and those from radioactive excitation by open circles. In Fig. 13, the solid line for the mean L-fluorescence yields represents Lay's data (La-34). The sharp break at $Z\approx 70$ in Fig. 13 represents the onset of the Coster–Kronig yield ($L_1 \rightarrow L_{2,3}M_{4,5}$) which is energetically forbidden for $50 \leq Z \leq 73$ (see Fig. 11). The existence of this sharp break has not been established experimentally. A break of this type does not appear in Fig. 12, where only the L_2 and L_3 subshells are ionized in the primary process. In Fig. 13, where excitation of the L_1 subshell makes a substantial contribution to the mean L-fluorescence yield, $\bar{\omega}_L$, such a break and increase in the fluorescence yield is expected.

Table VI summarizes experimental L-shell fluorescence yields following L-capture ω_{LL} (discussed in Sec. 1.3).

5.3. M-Shell Fluorescence Yields

Very little information is available about fluorescence yields in shells higher than the L shell. Six

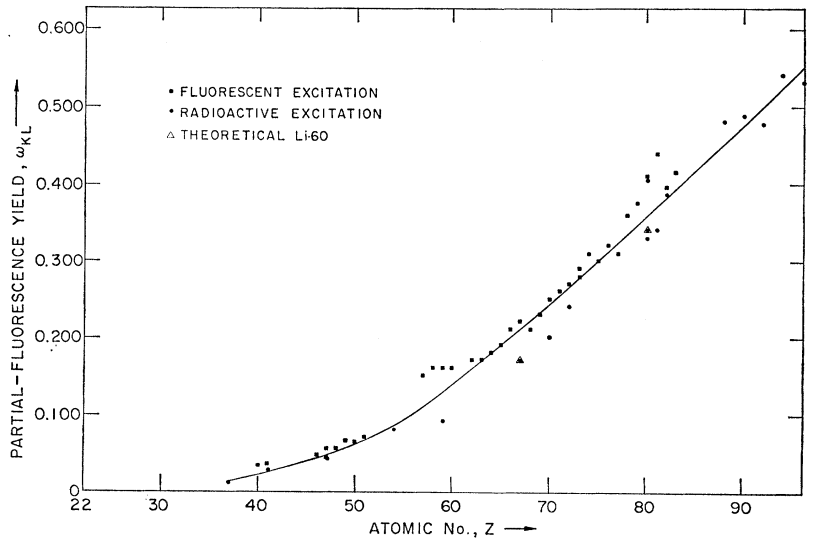

FIG. 12. The values of ω_{KL} as a function of atomic number are shown. The solid squares are measurements using photoexcitation of the K shell and the closed circles represent experiments in which the K shell was ionized by electron capture or internal conversion in radioactive decay.

TABLE V. Experimental mean L-shell fluorescence yields.

Z	Element	$\bar{\omega}_L$	Ref.	ω_{KL}	Ref.
23	V	0.00235±0.00025	Ko-60		
25	Mn	0.0029_5±0.0004	Ko-65		
29	Cu	0.0056	Ko-61		
31	Ga	0.0064±0.0004	Ko-60		
36	Kr	0.075	Bo-36		
	Kr	0.13	Au-25		
37	Rb	0.011±0.001	Ho-63		
	Rb			0.013±0.002	Ho-63
40	Zr	0.057	La-34	0.034±0.012	Jo-64b
41	Nb			0.022±0.002	Ho-63
	Nb			0.036±0.012	Jo-64b
42	Mo	0.067	La-34		
46	Pd			0.047±0.012	Jo-64b
47	Ag	0.047 (theory)	Li-60	0.045±0.003	Ho-63
	Ag			0.054±0.014	Jo-64b
	Ag			0.044±0.0003	Ho-64
	Ag	0.047±0.002	Be-59		
	Ag	0.029±0.003	Be-54		
	Ag	0.100	La-34		
48	Cd			0.055±0.014	Jo-64b
49	In			0.065±0.014	Jo-64b
50	Sn			0.064±0.014	Jo-64b
51	Sb			0.070±0.015	Jo-64b
	Sb	0.119	La-34		
52	Te	0.073±0.007	Ho-63		
		0.071 (theory)	Li-60		
	Te	0.122	La-34		
54	Xe	0.103±0.010	Fi-55		
	Xe	0.11±0.01	Ho-64		
	Xe	0.21	Bo-36		
	Xe			0.08±0.01	Ho-64
	Xe	0.25	Au-25		
56	Ba	0.148	La-34		
57	La	0.099 (theory)	Li-60	0.15±0.02	Jo-63
	La	0.092±0.007	Ho-63		
	La	0.158	La-34		
58	Ce			0.16±0.02	Jo-63
	Ce	0.163	La-34		
59	Pr			0.16±0.02	Jo-63
	Pr	0.167	La-34		
	Pr			0.09±0.01	Ho-64
60	Nd			0.16±0.02	Jo-63
	Nd	0.170	La-34		
62	Sm			0.17±0.01	Jo-63
	Sm	0.188	La-34		
63	Eu			0.17±0.01	Jo-63
	Eu	0.17	Bi-56		
64	Gd			0.18±0.02	Jo-63
	Gd	0.198	La-34		
65	Tb			0.19±0.01	Jo-63
	Tb			0.19	2-La-58
66	Dy	0.14±0.02	Zi-63		
	Dy			0.21±0.01	Jo-63
67	Ho			0.17±0.01	Ho-63
				0.17 (theory)	Li-60
	Ho			0.22±0.01	Jo-63
68	Er			0.21±0.03	Jo-63
	Er	0.228	La-34		
69	Tm			0.23±0.03	Jo-63
70	Yb			0.25±0.02	Jo-63
				0.20±0.02	Co-65
	Yb			0.20	2-La-58
71	Lu			0.26±0.03	Jo-63
72	Hf	0.260	La-34		
	Hf	0.17	2-Bi-56		
	Hf			0.24	2-La-58
	Hf			0.27±0.02	Jo-63
73	Ta			0.28±0.01	Ra-65a
				0.29±0.02	Jo-63
74	W	0.298	La-34		
	W			0.31±0.04	Jo-63
75	Re			0.30±0.04	Jo-63
76	Os	0.348	La-34		
	Os			0.32±0.04	Jo-63

TABLE V (*Continued*)

Z	Element	ω_L	Ref.	ω_{KL}	Ref.
77	Ir			0.31±0.04	Jo-63
78	Pt	0.348	La-34		
	Pt	0.32±0.02	Jo-62[a]		
	Pt			0.36±0.02	Jo-63
79	Au	0.365	La-34		
	Au			0.374±0.018	Jo-63
79	Au	0.430±0.012	La-65	0.287±0.04	La-65
80	Hg	0.410±0.040	Na-60		
	Hg	0.34±0.04	Sc-57		
	Hg	0.41±0.04	Le-62		
	Hg			0.34	2-La-58
	Hg	0.40±0.04	Ra-64		
	Hg	0.371±0.035	2-Ha-55	0.34 (theory)	Li-60
	Hg	0.24±0.05	Ja-54		
	Hg			0.33±0.02	Ho-63
	Hg			0.41±0.05	Jo-63
	Hg	0.39±0.06	Ra-64[a]		
	Hg			0.405±0.020	Ra-64
81	Tl	0.32±0.02	Wi-58		
	Tl	0.50±0.02	Bu-56		
	Tl	0.41±0.04	Ra-62		
	Tl	0.48±0.03	Ri-58		
	Tl			0.34	2-La-58
	Tl			0.44±0.05	Jo-63
82	Pb	0.39±0.02	Pa-57		
	Pb	0.398	La-34		
	Pb			0.385	2-La-58
	Pb			0.395±0.020	Jo-63
	Pb	0.36±0.02	Jo-62[a]		
83	Bi	0.38±0.02	Fi-57		
	Bi	0.38±0.04	Le-58		
	Bi	0.40±0.02	Wi-58		
	Bi	0.402	La-34		
	Bi	0.51±0.03	Bu-56		
	Bi			0.414±0.021	Jo-63
88	Ra			0.480±0.012	1-Ha-64
88	Ra	0.40±0.03	Gi-66		
	Ra	0.52±0.05	Bo-56		
90	Th			0.488±0.008	1-Ha-64
91	Pa	0.52±0.03	Ad-62[a]		
92	U			0.478±0.009	1-Ha-64
92	U	0.603±0.04	La-65	0.409±0.04	La-65
	U	0.45	La-34		
93	Np	0.66±0.08	Ak-64		
94	Pu			0.540±0.009	1-Ha-64
	Pu	0.486±0.01	Sa-61		
96	Cm			0.531±0.010	1-Ha-64

[a] ω_{LL} with $n_1, n_2, n_3 \approx 1.\ 0,\ 0.$

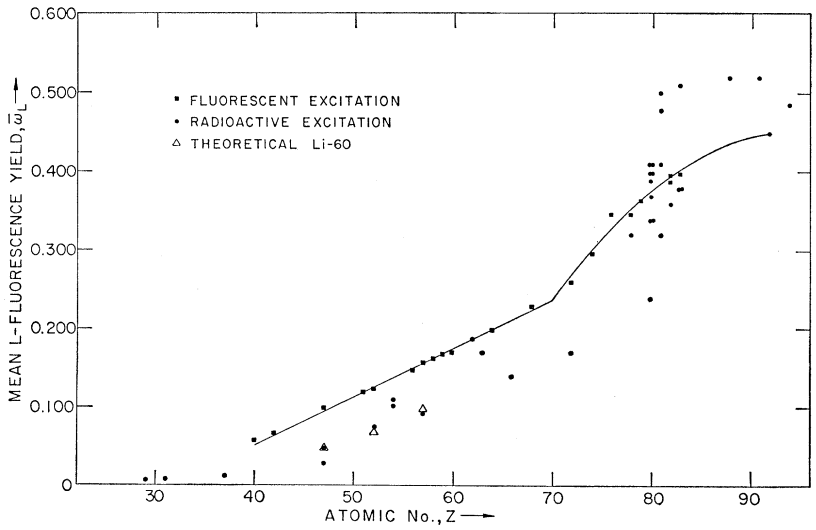

FIG. 13. The measured values of selected mean L-fluorescence yields, $\bar{\omega}_L$, are shown in this plot. The solid curve is drawn through the experimental points obtained by Lay (La-34).

measurements of mean M-fluorescence yields have been reported in the literature for elements between $Z=76$ and $Z=92$. The earliest measurement is that of Lay (La-34), who determined a mean M-fluorescence yield of uranium using photoionization of the M shell and photographic plates to measure the x-ray intensity (Sec. 4.2.1). Jaffe (Ja-54) has measured a mean M-shell fluorescence yield of bismuth by using the known M-shell conversion coefficient of the 46.5-keV transition following Pb^{210}(RaD) decay to compute the M-shell vacancies and then observed the M x rays with a proportional counter.

Finally, mean M-fluorescence yields of Os, Au, Pb, and Bi have been measured using the coincidence method with proportional counters, as described in Sec. 4.2.5. The mean M-shell yield measured in this way is designated ω_{LM} (in analogy with the similar quantity ω_{KL} defined for the L shell). It can be shown that ω_{LM} is approximately equal to a linear combination of the subshell fluorescence yields of the M_4 and M_5 subshells,

$$\omega_{LM}=0.4\omega_{M_4}+0.6\omega_{M_5}. \tag{33}$$

For a complete discussion of the procedure used to find Eq. (33), see Jo-65. Fluorescence yields for the M shell are summarized in Table VII.

The calculations of Ramberg and Richtmeyer (Ra-37) give the following values for M subshell fluorescence yields of gold ($Z=79$): $M_1=0.0050$, $M_2=0.0084$, $M_3=0.0045$, $M_4=0.017$, and $M_5=0.019$. These values when substituted into Eq. (33) for ω_{LM} give a somewhat lower value than that observed experimentally (Table VII).

5.4. Mesic X-Ray Fluorescence Yields

When fast negative mesons such as μ^-, π^-, or K^- have been slowed down to energies of a few eV, they can be captured into bound atomic orbits to form mesic atoms characterized by large values of the principal and orbital quantum numbers (n, 1~16). The wave functions of these states with high quantum numbers have little overlap with the nucleus. Before the meson can be captured by a nuclear proton, it must cascade down into a state of low atomic excitation having considerable overlap with the nucleus. In this cascade both radiative and Auger transitions occur. The theory of Fermi and Teller (Fe-47) indicates that the principal quantum numbers below which radiative transitions dominate over the Auger transitions, for example in nuclear emulsions, are $n\approx4.8$ for bromine and $n\approx5.6$ for silver. Wheeler (Wh-49) has calculated the Auger and mesic x-ray transition probabilities per unit time for the $2s\rightarrow2p$, $2s\rightarrow1s$, and $2p\rightarrow1s$ transitions in μ^- and π^- -mesic atoms, assuming a point-charge nucleus. The results of Wheeler's calculation show that for low Z, Auger electron emission is predominant for transitions depopulating the $2s$ level.

TABLE VI. L-shell fluorescence yields following L capture, ω_{LL}.

Z	Element	Value of ω_{LL} (experimental)	Ref.
73	Ta	0.23±0.01	Ra-65b
78	Pt	0.32±0.02	Jo-62
80	Hg	0.39±0.06	Ra-64
82	Pb	0.36±0.02	Jo-62
91	Pa	0.52±0.03	Ad-62

TABLE VII. Summary of mean M-shell fluorescence yields.

Z	Element	Experimental ω_{LM}	$\bar{\omega}_M$	Ref.
76	Os	0.016±0.003		Jo-65
79	Au	0.030±0.006		Jo-65
82	Pb	0.032±0.006		Jo-65
83	Bi	0.037±0.007		Jo-65
83	Bi		0.037±0.007	Ja-54
92	U		0.06	La-34

In addition to the theoretical studies, there also has been considerable experimental work reported for radiative transitions in μ^--mesic atoms in cosmic rays (Ch-54, Hi-51, Fa-52, Ha-53, 1-Bu-53) and with machine-produced muons (Fi-53, St-54, Ko-54, Co-64). Auger transitions in μ^--mesic atoms have been found in cosmic ray investigations (Co-49, 1-Fr-50, 2-Fr-50, Bo-51, Gr-51) and with machine-produced muons (Mo-53, Fr-53). Experimental evidence for radiative transitions (Ca-55, Sc-53, St-54, Mc-54) and for Auger electron emission (Me-50, Sa-62, Cu-62) in π^--mesic atoms has been obtained with machine-produced pions. In one investigation, the π^--mesic Auger yields were compared with those from K^--mesic atoms with the finding that the latter yields are about 75% larger than those from π^--mesic atoms in emulsions (Ch-58).

The experimental evidence shows that the Auger electrons from mesic atoms are emitted with quite low energies. In nuclear emulsion studies, the lower limit of detectability for electrons is about 14 keV. These low-energy electrons must arise from Auger transitions in silver and bromine associated with principal quantum numbers in the range of $n=4$ to 8, consistent with the theory of Fermi and Teller (Fe-47). Some of the higher energy (75–125 keV) Auger electrons observed may be due to $2s\rightarrow1s$ transitions in light elements such as carbon, nitrogen, and oxygen in the emulsions, assuming that the probability of cascade through the $2s$ state is not negligible. In low-Z elements (Be, B, C, N, O) the emission of Auger electrons predominates for transitions between states above $n=3$, below which the radiative transitions become important.

Once the meson has cascaded down to quantum states of low principal quantum number, capture by the nucleus competes strongly with radiative transitions in depleting these states. Finally, when the meson reaches the $1s$ state, it lives a relatively long time (of the order of 10^{-6} sec) before it is captured by the nucleus, as

compared to the time required for it to cascade down to the $1s$ state (generally less than 10^{-12} sec). Extensive calculations of the cascade time have been made (2-Bu-53, De-54, Jo-52). The fact of the long lifetime in the $1s$ state is convincing evidence that the interaction between muons and nucleons is weak (Wh-49).

Since the radii of mesic orbits are some 200 times smaller than the electron orbits for the same principal quantum number, mesic orbits below about $n=3$ in low Z elements and about $n=5$ for middle Z elements lie wholly within the radius of the K-electron orbit where the mean electron density is so small that Auger transitions become negligible. For this reason the mesic x-ray fluorescence yields for transitions between quantum states of low principal quantum number are close to unity, with the exception of the $2s\rightarrow 1s$ transition, for which the radiative transition is absolutely forbidden. Good evidence, both experimental and theoretical, exists that low-Z elements such as Be, B, C, N, O, Mg, Al, give one K-mesic x ray for each stopping muon or pion.

It may be noted that in addition to radiative transitions and direct capture of the meson by the nucleus, the two principal processes depopulating states of low quantum number, other effects also occur. One such effect is a process by which the muon, bound in a $3d$ orbit in a very heavy element (Th, U), makes a nonradiative transition to the $1s$ state accompanied by an $E2$ Coulomb excitation of a nuclear energy state. This process may have a transition probability large enough to cause a significant decrease in the yield of $3d\rightarrow 2p$ and $2p\rightarrow 1s$ mesic x rays (2-Ru-62, Ki-62, Fo-60). It has been found that the K mesic x-ray yields per stopped muon from Th^{232}, U^{235}, and U^{238} are, respectively, 15, 29, and 23% lower than that from lead (Mu-60). Thus the $3d\rightarrow 1s$ nonradiative transition of the muon, with the energy going to excite an $E2$ transition in the nucleus, may compete significantly in heavy elements with the radiative $3d\rightarrow 2p$ and $2p\rightarrow 1s$ cascade.

As newer accelerators, capable of producing very high fluxes of mesons ("meson factories") come into operation, further studies of the details of the deexcitation of the atomic states of mesic atoms will become feasible. As the mesic x rays have much higher energies than the corresponding x rays from electronically excited atoms, the study of the fluorescence yields and of Auger transitions might be extended to the M, N, etc. shells with detailed measurements of the yields from these higher shells in mesic atoms.

ACKNOWLEDGMENTS

The authors are grateful to their colleagues in this field for supplying some of their data before publication. We would also like to express our thanks to Dr. T. C. Merkle for his continued support and encouragement. This work was supported by the U.S. Atomic Energy Commission.

6. LIST OF REFERENCES

This is a complete list of references for all relevant material up to 10 May 1966.

Ac-60 G. D. Achard, *Proceedings of the Second Symposium on X-Ray Microscopy and Microanalysis* (Elsevier Publishing Co., Ltd., Amsterdam, 1960), pp. 331.

Ad-62 A. M. Adamson, M. Duquesne, and R. Foucher, J. Phys. Radium **23,** 580 (1962).

Ak-64 G. G. Akalaev, N. A. Vartanov, and P. S. Samoilov, Izv. Akad. Nauk SSSR, Ser. Fiz. **28,** 1158, 1259 (1964) [Bull. Acad. Sci. USSR, Phys. Columbia Tech. Transl. **28,** 1260 (1964)].

Al-61 R. G. Albridge and J. M. Hollander, Nucl. Phys. **27,** 554 (1961).

Ar-35 E. Arends, Ann. Physik **22,** 281 (1935).

As-59 W. N. Asaad, Proc. Roy. Soc. (London) **A249,** 555 (1959). Nucl. Phys. **66,** 494 (1965); **63,** 337 (1965).

Au-25 P. Auger, J. Phys. Radium **6,** 205 (1925).

Ba-63 J. N. Bahcall, Phys. Rev. **132,** 362 (1963).

Ba-65 W. Bambynek, E. De Roost, A. Spernol, W. Van Der Eijk, and P. Vaninbrouk, Euratom Rept. EUR-2524.e (1965) (unpublished).

Be-30 H. Bethe, Ann. Physik **5,** 325 (1930).

Be-33 H. Bethe, in *Handbuch der Physik* (Julius Springer-Verlag, Berlin, 1933), Vol. 24, p. 273ff.

Be-54 G. Bertolini, A. Bisi, Lazarrini, and L. Zappa, Nuovo Cimento **11,** 539 (1954).

Be-55 I. Bergström, in *Beta- and Gamma-Spectroscopy,* edited by I. Bergström, (1955); and I. Bergström and C. Nordling, in *Alpha-, Beta-, and Gamma-Spectroscopy,* edited by K. Siegbahn (North-Holland Publishing Co., Amsterdam, 1964), p. 1523ff.

Be-64

Be-59 F. Bertrand, G. Charpak, and F. Suzor, J. Phys. Radium **20,** 956 (1959); **20,** 462 (1959).

1-Bi-56 A. Bisi, E. Germagnoli, and L. Zappa, Nucl. Phys. **1,** 593 (1956).

2-Bi-56 A. Bisi, L. Zappa, and E. Zimmer, Nuovo Cimento **4,** 307 (1956).

Bo-36 J. C. Bower, Proc. Roy. Soc. (London) **A157,** 662 (1936).

Bo-51 A. Bonetti and G. Tomasini, Nuovo Cimento **8,** 693 (1951).

Bo-56 E. Booth, L. Madansky, and F. Rasetti, Phys. Rev. **102,** 800 (1956).

Br-53 C. Broyles, D. Thomas, and S. Haynes, Phys. Rev. **89,** 715 (1953).

Br-58 H. Brysk and M. E. Rose, Rev. Mod. Phys. **30,** 1169 (1958); and ORNL-1830 (1955).

Br-59 V. Brabets, K. Gromov, B. Dzhelepov, and V. Morozov, Bull. Acad. Sci. USSR, Columbia Tech. Transl. **23,** 805 (1959).

Bu-35 E. H. S. Burhop, Proc. Roy. Soc. (London) **A148,** 272 (1935).

Bu-52 E. H. S. Burhop, *The Auger Effect and Other Radiationless Transitions* (Cambridge University Press, Cambridge, England, 1952).

1-Bu-53 F. D. S. Butement, Phil. Mag. **44,** 208 (1953).

2-Bu-53 G. R. Burbridge and A. H. DeBorde, Phys. Rev. **89,** 189 (1953).

Bu-55 E. H. S. Burhop, J. Phys. Radium **16,** 625 (1955).

Bu-56 J. Burde and S. G. Cohen, Phys. Rev. **104,** 1085 (1956).

Bu-58 A. O. Burford and S. K. Haynes, Bull. Am. Phys. Soc. **3,** No. 3, 208 (1958).

Ca-55 M. Camac, A. D. McGuire, J. B. Platt, and H. J. Schulte, Phys. Rev. **99,** 897 (1955); **88,** 134 (1952).

Ca-61 E. J. Callan, Phys. Rev. **124,** 793 (1961).

Ca 63a E. J. Callan, Rev. Mod. Phys. **35,** 524 (1963).

Ca-63b E. J. Callan, preprint (1963) (unpublished); Bull. Am. Phys. Soc. **7,** N416 (1962).

Cam-63 A. J. Campbell, Proc. Roy. Soc. (London) **A274,** 319 (1963).

Ch-54 W. Y. Chang, Rev. Mod. Phys. **21,** 133 (1949); Phys. Rev. **95,** 1288 (1954).

Ch-58 E. B. Chesick and J. Schnepps, Phys. Rev. **112,** 1810 (1958).

Co-35 D. Coster and R. Kronig, Physica **2,** 13 (1935).

Co-49 M. G. E. Cosyns, C. C. Dilworth, G. P. S. Occhialini, M. Schoenberg, and N. Page, Proc. Phys. Soc. (London) **A62,** 801 (1949).

Co-58 A. J. Cochran and M. A. S. Ross, Proc. Phys. Soc. (London) **A71,** 1011 (1958).

Co-64 R. C. Cohen, S. Devons, and A. D. Kanaris, Nucl. Phys. **57,** 255 (1964).

Co-65 G. D. Cole and A. Mukerji, Bull. Am. Phys. Soc. **10,** No. 2, 262 (1965).

Cu-49 S. C. Curran, J. Angus, and A. L. Cockcroft, Phil. Mag. **40,** 36, 929 (1949).

Cu-62 J. E. Cuevas, M.S. thesis, Marquette University, Milwaukee, Wisconsin (1962).

Da-64 C. M. Davisson, in *Alpha-, Beta-, and Gamma-Spectroscopy,* edited by K. Siegbahn (North-Holland Publishing Co., Amsterdam, 1964), p. 37ff.

De-54 A. H. deBorde, Proc. Phys. Soc. (London) **A67,** 57 (1954).

Di-63 J. S. Dionisio, Ann. Phys. (Paris) **8,** 747 (1963); and thesis (Paris) (1963).

Dr-57 R. W. P. Drever and A. Moljk, Phil. Mag. **2,** 427 (1957).

Dy-62 B. B. D'yakov and I. M. Rogachev, Izv. Akad. Nauk SSSR, Ser. Fiz. **26,** 191 (1962) [Bull. Acad. Sci. USSR Columbia Tech. Transl. Phys. **26,** 191 (1962)].

Er-61 P. Erman and Z. Sujkowski, Arkiv Fys. **20,** 209 (1961).

Fa-52 A. Farfarman and M. H. Schamos, Phys. Rev. **87,** 219 (1952).

Fa-57 J. A. V. Fairbrother, D. G. Parkyn, and B. M. O'Connor, Proc. Phys. Soc. (London) **A70,** 262 (1957).

Fe-47 E. Fermi and E. Teller, Phys. Rev. **72,** 399 (1947); cf. also B. Feretti, Nuovo Cimento **5,** 325 (1948).

Fe-65 J. G. Ferreira, M. O. Costa, M. I. Goncalves, and L. Salgueiro, J. Phys. (Paris) **26,** 5 (1965).

Fi-53 V. Fitch and J. Rainwater, Phys. Rev. **92,** 789 (1953).

Fi-55 R. W. Fink and B. L. Robinson, Phys. Rev. **98,** 1293 (1955).

Fi-57 R. W. Fink, Phys. Rev. **106,** 266 (1957).

Fo-59 R. N. Forest and H. T. Easterday, Phys. Rev. **112,** 950 (1959).

Fo-60 B. Forkman and S. A. E. Johansson, Nucl. Phys. **20,** 136 (1960).

1-Fr-50 C. Franzinetti, Phil. Mag. **41,** 86 (1950).

2-Fr-50 W. F. Fry, Phys. Rev. **79,** 893 (1950).

Fr-53 W. F. Fry, Nuovo Cimento **10,** 490 (1953).

Fr-58 W. F. Frey, R. E. Johnston, and J. I. Hopkins, Phys. Rev. **113,** 1057 (1958); Bull. Am. Phys. Soc. **3,** No. 4, 299 (1958); TID-14854 (1958).

Ge-37 F. Genevese, M. S. Livingston, and E. J. Konopinski, Phys. Rev. **51,** 835 (1937).

Ge-59 C. Greffrion and G. Nadeau, Air Force Office of Scientific Res. Report TR-59-145 (1959) (unpublished).

Gi-66 F. B. Gil, C. F. Miranda, J. S. Lobo, and J. G. Ferreira, Port. Phys. **4,** 17 (1965) (in Portuguese); Nuclear Sci. Abstr. **20,** 10075 (1966).

Go-61 C. Godeau, Natl. Bur. Std. Tech Note No. 91 (1961) (unpublished).

Gr-51 G. Groetzinger, L. B. Leder, and F. L. Ribe, Phys. Rev. **81,** 626 (1951).

Gr-56 P. R. Gray, Phys. Rev. **101,** 1306 (1956); and AEC Report UCRL-3104 (1955).

Gr-61a R. L. Graham and J. S. Merritt, Can. J. Phys. **39,** 1058 (1961).

Gr-61b R. L. Graham, F. Brown, G. T. Ewan, and J. Uhler, Can. J. Phys. **39,** 1086 (1961).

Ha-53 G. G. Harris and T. J. B. Shanley, Phys. Rev. **89,** 983 (1953).

1-Ha-55 G. R. Harrison, R. C. Crawford, and J. I. Hopkins, Phys. Rev. **99,** 1629A (1955); Phys. Rev. **100,** 841 (1955).

2-Ha-55 S. K. Haynes and W. T. Achor, J. Phys. Radium **16,** 635 (1955).

Ha-57 H. L. Hagedoorn and J. Konijn, Physica **23,** 1069 (1957).

Ha-60 H. L. Hagedoorn and A. H. Wapstra, Nucl. Phys. **15,** 146 (1960).

1-Ha-64 J. W. Halley and D. Engelkemeir, Phys. Rev. **134,** A24 (1964).

2-Ha-64 S. Hagström, C. Nordling, and K. Siegbahn, in *Alpha-, Beta-, and Gamma-Spectroscopy,* edited by K. Siegbahn (North-Holland Publishing Co., Amsterdam, 1964), Appendix 2.

He-55 J. Heintze, Z. Physik **143,** 153 (1955); Z. Naturforsch. **9a,** 469 (1954).

Hi-51 E. P. Hincks, Phys. Rev. **81,** 313 (1951).

Ho-58 D. Hoffman and B. Dropesky, Phys. Rev. **109,** 1211 (1958).

Ho-63 K. Hohmuth, G. Müller, and J. Schintlmeister, Nucl. Phys. **48,** 209 (1963).

Ho 64 K. Hohmuth and G. Winter, Phys. Letters **10,** 58 (1964) and private communication (1964).

Ja-54 A. A. Jaffe, Bull. Res. Council (Israel) **3,** No. 4, 316 (March 1954); [see Phys. Abstr. **58,** 360, No. 2782 (1955)].

Jo-52 B. L. Jaffe and I. Ya. Pomeranchuk, Zh. Eksperim. i Teor. Fiz. **23,** 123 (1952).

Jo-60 B. R. Joshi, Proc. Phys. Soc. (London) **A77,** 1205 (1960).

Jo-61 R. C. Jopson, H. Mark, C. D. Swift, and J. H. Zenger, Phys. Rev. **124,** 157 (1961).

Jo-62 R. C. Jopson, H. Mark, and C. D. Swift, Phys. Rev. **127,** 1612 (1962).

Jo-63 R. C. Jopson, H. Mark, C. D. Swift, and M. A. Williamson, Phys. Rev. **131,** 1165 (1963); Bull. Am. Phys. Soc. **8,** No. 1, 49 (1963); **7,** 491 (1962).

Jo-64a R. C. Jopson, J. M. Khan, H. Mark, C. D. Swift, and M. A. Williamson, Phys. Rev. **133,** A381 (1964); Bull. Am. Phys. Soc. **9,** No. 1, 51 (1964).

Jo-64b R. C. Jopson, H. Mark, C. D. Swift, and M. A. Williamson, Phys. Rev. **136,** A69 (1964).

Jo-65 R. C. Jopson, H. Mark, C. D. Swift, and M. A. Williamson, Phys. Rev. **137,** A1353 (1965).

Ke-56 B. Kettele, H. Thomas, and A. Brosi, Phys. Rev. **103,** 190 (1956).

Ki-48a B. B. Kinsey, Can. J. Res. **A26,** 404 (1948).

Ki-48b B. B. Kinsey, Can. J. Res. **A26,** 421 (1948).

Ki-62 Y. N. Kim, Phys. Letters **3,** 33 (1962).

Kn 65 J. W. Knowles, in *Alpha-, Beta-, and Gamma-Spectroscopy,* edited K. Siegbahn (North-Holland Publishing Co., Amsterdam, 1964), p. 203ff.

Ko-54 S. Koslov, V. Fitch, and J. Rainwater, Phys. Rev. **95,** 291, 625 (1954).

Ko-58a J. Konijn, H. L. Hagedoorn, and B. van Nooyen, Physica **24,** 129 (1958).

Ko-58b J. Konijn, B. van Nooyen, and H. L. Hagedoorn, Physica **24,** 377 (1958).

Ko-60 A. A. Konstantinov, T. E. Sazonova, and V. V. Perepelkin, Izv. Akad. Nauk SSSR, Ser. Fiz. **24,** 1480 (1960) [Bull. Acad. Sci. USSR, Phys., Columbia Tech. Transl. **24,** 1472 (1960)].

Ko-61 A. A. Konstantinov, I. A. Sokolova, and T. E. Sazonova, Izv. Akad. Nauk SSSR, Ser. Fiz. **25,** 228 (1961) [Bull. Acad. Sci. USSR, Phys., Columbia Tech. Transl. **25,** 219 (1961)].

Ko-64 A. A. Konstantinov, V. V. Perepelkin, and T. E. Sazonova, Izv. Akad. Nauk SSSR, Ser. Fiz. **28,** 107 (1964) [Bull. Acad. Sci. USSR, Phys., Columbia Tech. Transl. **28,** 103 (1964)].

Ko-65 A. A. Konstantinov and T. E. Sazonova, Izv. Akad. Nauk SSSR, Ser. Fiz. **29,** 302 (1965) [Bull. Acad. Sci. USSR, Phys. Columbia Tech. Transl. **29,** 305 (1965)].

Kr-61 P. Kramer, thesis, Amsterdam (1961).

Kr-62 P. Kramer, A. De Beer, E. C. Bos, and J. Blok, Physica **28,** 582 (1962).

Kü-35 H. Küstner and E. Arends, Ann. Physik **22,** 443 (1935).

La-34 H. Lay, Z. Physik **91,** 533 (1934).

La-56a J. Laberrigue and P. Radvanyi, J. Phys. Radium **17,** 944 (1956); Compt. Rend. **242,** 901 (1956).

La-56b J. Laberrigue-Frolow, P. Radvanyi, and M. Langevin, J. Phys. Radium **17**, 530 (1956).

1-La-58 W. Laskar, Ann. Physique **3**, 258 (1958).

2-La-58 N. H. Lazar and W. S. Lyon, Bull. Am. Phys. Soc. **3**, No. 1, 29 (1958); and private communication (1958).

La-65 M. A. D. Lazzaro and G. Missoni, Istituto di Superiore di Sanita; Laboratori di Fisica Report (in English) ISS-65/11, Rome, Italy (1965) (unpublished).

Le-53 H. W. Lewis, B. E. Simmons, and E. Merzbacher, Phys. Rev. **91**, 943 (1953); **95**, 83 (1954).

Le-58 N. K. Lee, thesis, Vanderbilt Univ., Report TID-14963 (1958) (unpublished).

Le-62 H. Leutz and K. Ziegler, Z. Physik **166**, 582 (1962).

Le-65 M. Leistner and K. Friedrich, Atomkernenergie **8**, 311 (1965).

Li-60 M. A. Listengarten, Izv. Akad. Nauk SSSR, Ser. Fiz. **24**, 1041 (1960) [Bull. Acad. Sci. USSR, Phys. **24**, 1050 (1960)].

Li-62 M. A. Listengarten, Izv. Akad. Nauk SSSR, Ser. Fiz. **26**, 182 (1962) [Bull. Acad. Sci. USSR, Phys., Columbia Tech. Transl. **26**, 182 (1962)]; Izv. Akad. Nauk SSSR, Ser. Fiz. **25**, 792 (1961) [Bull. Acad. Sci. USSR, Phys., Columbia Tech. Transl. **25**, 803 (1961)].

Ma 36 H. S. W. Massey and E. H. S. Burhop, Proc. Roy. Soc. (London) **A153**, 661 (1936).

Ma 64 Hans Mark, Nucl. Instr. Methods **28**, 131 (1964).

Mc 54 A. D. McGuire, M. Camac, M. L. Halbert, and J. B. Platt, Phys. Rev. **95**, 625 (1954).

Me 50 M. G. K. Menon, H. Muirhead, and O. Rochat, Phil. Mag. **41**, 583 (1950).

Me-65 W. Mehlhorn, Phys. Letters **15**, 46 (1965); Z. Physik **187**, 21 (1965).

Mo-53 H. Morinaga and W. F. Fry, Nuovo Cimento **10**, 308 (1953).

1-Mo-61 E. Morrand and A. Moussa, Nucl. Phys. **25**, 292 (1961).

2-Mo-61 R. B. Moler and R. W. Fink, Bull. Am. Phys. Soc. **6**, No. 5, 428 (1961).

Mo-63 R. B. Moler and R. W. Fink, Phys. Rev. **131**, 821 (1963).

Mu-60 A. I. Muhkin, M. J. Balatz, L. N. Kondratiev, L. G. Landsburg, P. I. Lebedev, Yu. V. Obukliov, and B. Pontecorvo, *Proceedings of the High Energy Physics Conference, Rochester, 1960* (Interscience Publishers, Inc., New York, 1960), p. 550.

Na-60 J. C. Nall, Q. L. Baird, and S. K. Haynes, Phys. Rev. **118**, 1278 (1960).

Pa-57 E. T. Patronis, Jr., C. H. Braden, and L. D. Wyly, Phys. Rev. **105**, 681 (1957).

Pa-59 L. G. Parratt, Rev. Mod. Phys. **31**, 616 (1959).

Pä-63 R. Päschke, Z. Physik **176**, 143 (1963).

Pe-61 L. Persson and Z. Sujkowski, Arkiv Fys. **19**, 309 (1961).

Pi-35 L. Pincherle, Nuovo Cimento **12**, 81 (1935).

Ra-37 E. G. Ramberg and F. K. Richtmeyer, Phys. Rev. **51**, 913 (1937).

Ra-61 J. Ravier, P. Marguin, and A. Moussa, J. Phys. Radium **22**, 249 (1961).

Ra-62 M. K. RamaSwamy, Nucl. Phys. **33**, 320 (1962); Bull. Am. Phys. Soc. **7**, No. 4, 342 (1962).

Ra-64 P. V. Rao and B. Crasemann, Bull. Am. Phys. Soc. **9**, No. 7, 720 (1964).

Ra 65a P. V. Rao and B. Crasemann, Phys. Rev. **137**, B64 (1965); Bull. Am. Phys. Soc. **9**, No. 4, 396 (1964).

Ra-65b P. V. Rao and B. Crasemann, Phys. Rev. **142**, 768 (1966); Bull. Am. Phys. Soc. **10**, No. 5, 589 (1965); and private communication (1965).

RF-55 B. L. Robinson and R. W. Fink, Rev. Mod. Phys. **27**, 424 (1955).

RF-60 B. L. Robinson and R. W. Fink, Rev. Mod. Phys. **32**, 117 (1960).

Ri-58 K. Risch, Z. Physik **150**, 87 (1958).

Ri-59 R. A. Rightmire, J. R. Simanton, and T. P. Kohman, Phys. Rev. **113**, 1069 (1957); R. A. Rightmire, thesis, Carnegie Tech., Report NYO-6633 (1952).

Ri-60 K. Risch, Z. Physik **159**, 89 (1960).

Ro-55 M. A. S. Ross, A. J. Cochran, J. Hughes, and N. Feather, Proc. Phys. Soc. (London) **A68**, 612 (1955).

Ro 57 C. E. Roos, Phys. Rev. **105**, 931 (1957); **100**, 1267 (1955); **93**, 401 (1954); Bull. Am. Phys. Soc. **30**, No. 7, 40 (1955).

Ro-59 C. E. Roos, private communication to B. L. Robinson, quoted in RF-60 (1959).

Ru-55 R. A. Rubenstein and J. N. Snyder, Phys. Rev. **97**, 1653 (1955).

1-Ru-62 M. A. Rumsh and V. N. Shchemelev, Zh. Eksperim. i Teor. Fiz. **42**, 727 (1962) [English transl.: Soviet Phys.—JETP **15**, 507 (1962)].

2-Ru-62 J. E. Russell, Phys. Rev. **127**, 245 (1962).

Sa-61 L. Salgueiro, J. G. Ferreira, J. J. H. Park, and M. A. S. Ross, Proc. Phys. Soc. (London) **77**, 657 (1961).

Sa-62 J. Sacton, thesis, quoted in Cu-62.

Sc-53 H. J. Schulte, J. B. Platt, and M. Camac, Phys. Rev. **89**, 905 (1953).

Sc-57 H. Schmied and R. W. Fink, Phys. Rev. **107**, 1062 (1958).

Si 64 K. Siegbahn, *Alpha-, Beta-, Gamma-Spectroscopy* (North-Holland Publishing Co., Amsterdam, 1964), p. 79ff.

St-37 R. J. Stephenson, Phys. Rev. **51**, 637 (1937).

St-54 M. B. Sterns, S. DeBenedetti, M. Sterns, and L. Leipuner, Phys. Rev. **93**, 1123 (1954); **95**, 625, 1353; **96**, 804 (1954); **97**, 240 (1955).

Su-61a Z. Sujkowski and O. Melin, Arkiv Fys. **20**, 193 (1961).

Su-61b Z. Sujkowski, Arkiv Fys. **20**, 243 (1961).

Su-62 T. Suter and P. Reyes Suter, Arkiv Fys. **20**, 393 (1962).

Ta-63 J. G. V. Taylor and J. S. Merritt, Proc. Conf. *Atomic Electrons in Nuclear Transformations*, Warsaw, Poland, Vol. III, 465 (1963).

To-58 J. Tousset and A. Moussa, J. Phys. Radium **19**, 39 (1958).

Va-62 J. Valentin, Compt. Rend. **254**, 858 (1962).

Vi-61 C. Victor, Ann. Phys. (Paris) **6**, 183 (1961).

Wa-59 A. Wapstra, G. Nijgh, and R. van Lieshout, *Nuclear Spectroscopy Tables* (North-Holland Publishing Co., Amsterdam, 1959).

Wa-61 R. E. Watson and A. J. Freeman, Phys. Rev. **123**, 521 (1961); **124**, 1117 (1961); **118**, 1036 (1960); and MIT Tech. Rept. No. 12 (1959).

Wa-62 T. Wanabe, H. W. Schnopper, and F. N. Girillo, Phys. Rev. **127**, 2055 (1962) and Air Force Report, AFOSR-1932 (1961).

We-27 G. Wentzel, Z. Physik **43**, 524 (1927).

We-55 J. P. Welker and M. L. Perlman, Phys. Rev. **100**, 74 (1955).

Wh 49 J. A. Wheeler, Rev. Mod. Phys. **21**, 133 (1949).

Wi-58 H. Winkenbach, Z. Physik **152**, 387 (1958).

Zi-63 T. Zimmerli and A. Flammersfeld, Z. Physik **176**, 323 (1963).